HHS Public Access

Author manuscript

Curr Biol. Author manuscript; available in PMC 2024 October 09.

Published in final edited form as:

Curr Biol. 2023 October 09; 33(19): 4202–4216.e9. doi:10.1016/j.cub.2023.08.075.

Cep104 is a component of the centriole distal tip complex that regulates centriole growth and contributes to *Drosophila* spermiogenesis

John M. Ryniawec[1,3], **Matthew R. Hannaford**[2,3], **Melanie E. Zibrat**[1], **Carey J. Fagerstrom**[2], **Brian J. Galletta**[2], **Sophia E. Aguirre**[1], **Bethany A. Guice**[1], **Spencer M. Dean**[1], **Nasser M. Rusan**[2,*], **Gregory C. Rogers**[1,4,*]

[1]Department of Cellular and Molecular Medicine, University of Arizona Cancer Center, University of Arizona, Tucson, AZ, 85724, USA

[2]Cell and Developmental Biology Center, National Heart Lung and Blood Institute, National Institutes of Health, Bethesda, MD, USA

[3]These authors contributed equally

[4]Lead contact

SUMMARY

Proper centrosome number and function relies on the accurate assembly of centrioles, barrel-shaped structures that form the core duplicating elements of the organelle. Growth of centrioles is regulated in a cell cycle-dependent manner; while new daughter centrioles elongate during S/G2/M-phase, mature mother centrioles maintain their length throughout the cell cycle. Centriole length is controlled by synchronized growth of the microtubules that ensheath the centriole barrel. Although proteins exist that target the growing distal tips of centrioles, such as CP110 and Cep97, these proteins are generally thought to suppress centriolar microtubule growth, suggesting that distal tips may also contain unidentified counteracting factors that facilitate microtubule polymerization. Currently, a mechanistic understanding of how distal tip proteins balance microtubule growth and shrinkage to either promote daughter centriole elongation or maintain centriole length is lacking. Using a proximity-labeling screen in *Drosophila* cells, we identified Cep104 as a novel component of a group of evolutionarily conserved proteins that we collectively refer to as the Distal Tip Complex (DTC). We found that Cep104 regulates centriole growth and promotes centriole elongation through its microtubule-binding TOG domain.

*Correspondence: nasser@nih.gov (N.M.R.), gcrogers@arizona.edu (G.C.R).

AUTHOR CONTRIBUTIONS

JMR was the lead in designing, performing and analyzing all experiments involving cultured fly cells as well as manuscript preparation. MRH was the lead in designing, performing, and analyzing all experiments involving *in vivo* models as well as manuscript preparation. CJF and BJG performed Y2H experiments. MEZ, SEA, and BAG performed co-IPs for Cep97 fragments, CP110 fragments, and Klp10a fragments, respectively. SMD performed microtubule co-sedimentation assays. NMR and GCR contributed to project design, manuscript preparation and funding acquisition.

DECLARATION OF INTERESTS

The authors declare no competing interests.

Furthermore, analysis of Cep104 null flies revealed that Cep104 and Cep97 cooperate during spermiogenesis to align spermatids and coordinate individualization. Lastly, we mapped the complete DTC interactome and show that Cep97 is the central scaffolding unit required to recruit DTC components to the distal tip of centrioles.

eTOC Blurb

Ryniawec *et al.* investigate distal tip proteins that regulate centriole length. They find that Cep104 is a novel component that binds microtubules and promotes centriole elongation. Double mutation of Cep104 and Cep97 reveals unique roles for these proteins during *Drosophila* spermiogenesis. These findings provide insight into centriole assembly.

Keywords

centrosome; centriole; microtubule; axoneme; distal tip complex; spermiogenesis

INTRODUCTION

Centrosomes are cytoplasmic organelles that function as the major microtubule-organizing center of the cell and are used to construct various microtubule-based structures, such as mitotic spindles and cilia[1,2]. The centrosome is built around a pair of centrioles, barrel-shaped organelles composed of singlet, doublet, or triplet microtubules arranged in nine-fold radial symmetry[1,2]. While length of the centriole barrel can be highly variable between different cell-types within the same organism (ranging from ~0.18 μm in *Drosophila* embryos to ~1 μm in spermatocytes), centriole length is tightly regulated and consistent among cells of the same cell-type[3]. Controlling centriole length is critical, as the centriole's structure tunes the microtubule nucleation capacity of centrosomes and restricts centriole duplication to once per cell cycle, ensuring tight control of centrosome number[4–6]. However, mechanisms that define centriole length and regulate centriole elongation are poorly understood.

Centriole duplication begins during S-phase with the formation of a 'procentriole', a central cartwheel composed of Sas6 oligomers surrounded by nine triplet microtubules, near the surface of an existing mother centriole[1,2,7]. Procentrioles appear orthogonal to the proximal end of the mother centriole and are arranged such that the centriolar microtubule plus-(+) ends reside at the distal tip of the centriole[1,2,7,8]. During the elongation phase, net centriole growth is slow and processive, with the microtubules growing collectively and elongating the centriole barrel, and, although not as dramatic as cytoplasmic microtubules, centriole microtubules appear to be dynamic even within a mother centriole that has reached its terminal length[7–12].

Three evolutionarily conserved proteins localize to the distal tip of centrioles and control centriole length: Klp10a, Cep97, and CP110[10,13–16]. These components collaborate to promote the elongation of new daughter centrioles during G2/M-phase, while maintaining the length and planarity of the distal surface of mother centrioles throughout the cell cycle. *Drosophila* Klp10a (and human Kif24) are members of the kinesin-13 subfamily

of microtubule-depolymerases that prevent centriole over-elongation (or ciliogenesis, in the case of Kif24), reinforcing previous findings that centriolar microtubules are a key determinant of overall centriole length[4,10,17]. Cep97 and CP110 are well-established distal tip markers; Cep97 directly binds and recruits CP110 to centrioles and are generally thought to antagonize proteins that promote centriole elongation[13,14,16,18,19]. However, mutation of either *Drosophila* Cep97 or CP110 show opposite effects on centriole length when comparing different mutant tissues, suggesting that their activities are more intricate[14,16]. For example, centrioles in Cep97 null spermatocytes are longer than normal, but shorter in Cep97 or CP110 null mutant wing discs[16]. Moreover, Cep97 and CP110 suppress ciliogenesis by preventing growth of axonemal microtubules from the distal end of the centriole[18–21]. Thus, Cep97 and CP110 may suppress the elongation or shortening of centrioles in a cell-type specific manner and likely exert their effects at the plus-ends of centriolar microtubules. In addition to their effects on length of the centriole barrel, depletion or mutation of either Cep97, CP110, or Klp10a cause spurious growth of long individual microtubules that extend from the centriole distal tip in non-ciliated cells[10,15,17,22].

These results have led to a model where Cep97 and CP110 form a “protective cap” at the distal tip to suppress centriolar microtubule growth but is porous enough to allow Klp10a limited access to microtubule plus-ends[10,13]. How the activities of these seemingly negative growth regulators are coordinated to allow centriole elongation is still unclear. Here, we identify Cep104 as a new, functionally important member of a complex we call the Distal Tip Complex (DTC), whose components act in a coordinated manner to control centriole length. Specifically, Cep97 binds and recruits Cep104 to the distal tip to promote centriole elongation through its microtubule-binding Tumor-Overexpressed Gene (TOG) domain. This behavior is particularly apparent during spermatogenesis when Cep104 cooperates with Cep97 in producing functional sperm.

RESULTS

Drosophila CG10137 is a homolog of human Cep104

To identify new regulators of centriole length, we performed a BioID proximity-labeling screen in cultured *Drosophila* S2 cells using Cep97 tagged with the promiscuous biotin ligase, miniTurbo[23,24]. V5-Cep97-miniTurbo localized as one or two distinct spots at Pericentrin-like protein (Plp)-labeled centrioles and covalently tagged proteins in proximity to distal tips, as detected with fluorescently-tagged streptavidin (Figures S1A and S1B). By performing tandem mass spectrometry on streptavidin-bead pulldowns, we identified 262 proteins enriched (and 22 unique) when compared to cytoplasmic miniTurbo expressing cells, including the structural centriole proteins Sas4 and Ana2 which likely appear near the distal tip during procentriole assembly (Data S1). As expected, Cep97 and CP110 were highly enriched, as was Klp10a, an established CP110-binding protein[10] (Figure S1C). We also identified an uncharacterized gene, CG10137, encoding a homolog of human (Hs) Cep104. Notably, Cep104 is required for proper cilia formation and resides at the centriole distal tip in cycling human cells[25,26]. Alignment of homologs from a variety of species revealed high sequence similarity and a general similarity in functional domain composition

and arrangement, suggesting that Cep104 is an evolutionarily conserved protein. *Drosophila* (Dm) Cep104 contains an N-terminal Jelly Roll/IFT25/APC10-like domain, an adjacent coiled-coil, a microtubule- or tubulin-binding TOG domain, and a C-terminal zinc finger (Figures 1A, S2A, and S2B)[25,27–29]. Interestingly, DmCep104 lacks the C-terminal EB1-binding SxIP motif found in its vertebrate homologs (Figure S2B), and live imaging of GFP-Cep104 in S2 cells revealed that it does not track on microtubule plus-ends with TagRFP-EB1, unlike HsCep104 (Figure S2C; Video S1)[25,30].

DmCep104 is recruited to the distal tip of centrioles during procentriole assembly

Previous proteomic screening identified Cep104 as a constituent of human centrosomes and was later shown to directly bind both Cep97 and CP110 and co-localize with CP110 at the distal tips of centrioles in human cells[25,31,32]. While Cep104 is known to regulate the architecture of microtubules at the tips of ciliary and flagellar axonemes[33,34], it is unknown whether Cep104 affects microtubules at centriole distal tips and/or regulates centriole length. To examine whether the centriole distal tip is a conserved site of Cep104 localization, we generated antibodies to all four centriole distal tip proteins (Cep97, CP110, Klp10a, and Cep104), and examined their distributions in S2 cells. Antibody specificity was validated using both immunoblotting and immunostaining in RNAi-treated S2 cells (Figures S3A–D and S3A'–C'). As expected, Cep97 and CP110 localized as spots at the distal tips of Plp-stained centrioles (Figures S3A and S3B); Plp marks the surface of mature mother centrioles but not newly assembled daughters. Klp10a also appeared on centrioles as distinct spots and globally decorated microtubules in a punctate pattern, however, its centriole localization was relatively weak and variable (Figure S3C). Antibodies against Cep104 failed to detect the endogenous protein by Western blotting or immunostaining but specifically recognized transgenic GFP-Cep104 (Figures S3D and S3E), suggesting that endogenous Cep104 is a low abundance protein, although still detectable by BioID. GFP-Cep104 localized as either one or two distinct spots on Plp or Asterless (Asl)-stained centrioles (Asl also exclusively coats the surface of mature centrioles) (Figures 1B and S3E). Using 3D-Structured Illumination Microscopy (3D-SIM), we found that GFP-Cep104 co-localized with Cep97 and CP110 on centriole distal tips (Figures 1C and 1D).

Although Cep97 and CP110 appear sometime after procentriole assembly[35,36], it is unclear when during a canonical cell cycle that distal tip proteins are first recruited to centrioles. Using Fly-FUCCI, a fluorescent cell cycle reporter[37], we found that Cep97, CP110 and Cep104 all appear on procentrioles concurrently near the G1/S-phase transition as measured by their near complete shift from one to two centriole-associated spots between G1- and S-phases (Figure 1E)[37]. Similarly, when S-phase cells were identified using EdU incorporation, nearly all centrioles had duplicated and were associated with two distal tip spots (Figure 1F). The EdU-negative population consisted of both G1- and G2/M-phase cells (roughly 1:1) with centrioles that had either one or two distal tip spots, as expected. We conclude that Cep97, CP110 and Cep104 are recruited to distal tips soon after procentriole initiation where they remain throughout the cell cycle. Additionally, the centriole localization patterns of Cep97-CP110-Cep104 can be used as reliable markers in determining cell cycle stage in proliferating fly cells.

Cep104 promotes centriole elongation

Depletion of distal tip proteins triggers ciliogenesis in most model cell lines[13,17–21,38–40]. However, S2 cells do not form primary cilia and, therefore, offer an attractive system to study the functions of these proteins in regulating centriole length independent of ciliogenesis. Depletion of Cep97 or CP110 in S2 cells led to centriole shortening, and near elimination (Figure S3F), reportedly due to Klp10a-mediated microtubule depolymerization[10]. In contrast, centriole number increased after Klp10a depletion (Figure S3F), reportedly due to fragmentation of excessively elongated centrioles[10,22]. While we were unable to verify depletion of endogenous Cep104 by Western blot, we confirmed RNAi efficiency using RT-PCR, which eliminated the endogenous Cep104 mRNA (Figure 2A, upper panel). Moreover, Cep104 RNAi eliminated transgenic Cep104-GFP (Figure 2A, lower panel). Unlike Cep97 or CP110, Cep104 depletion did not lead to centriole loss and, in fact, Cep97 was retained on centriole tips (Figures 2B). Therefore, we used 3D-SIM to measure the distance between the mother Cep97 spot and the procentriole's Cep97 spot as a proxy for the length of centrioles (Figure 2C). Compared to centrioles in control cells, Cep104 depletion significantly decreased the distance between Cep97 spots (Figure 2D and 2E). As a more direct measure of centriole length, we also immunostained cells for Spd2 which labels the microtubule wall of the mother centriole barrel[10], appearing as parallel stripes in longitudinal section (Figure 2F). Restricting length measurements to those centriole pairs strictly oriented in longitudinal configuration also showed that the distance between Cep97 spots decreased in Cep104-depleted cells (Figures 2G and 2H). Likewise, longitudinal measurements of Spd2 length showed a significant shortening in mother centriole length in Cep104-depleted cells (Figure 2I), validating the use of Cep97 spots as a proxy for centriole length.

To test Cep104's role in centriole growth *in vivo*, we generated *cep104* null flies using CRISPR/Cas9 genome editing which was confirmed by PCR (Figure 2J). As in S2 cells, Cep97 was present on centrioles in *cep104* null somatic cells of the third instar larval wing disc (Figure 2K). However, centriole lengths within these mutant cells were unchanged compared to wild-type controls (Figures 2L and 2M). Thus, our findings suggest that Cep104 is required for proper centriole growth in some, but not all somatic cells, and acts through a mechanism distinct from Cep97 and CP110 as evident by their phenotypic differences.

Cep104 promotes centriole elongation through its microtubule-binding TOG domain

We next sought to understand how Cep104 promotes centriole growth. Since Cep104 contains a microtubule-binding TOG domain, we hypothesized that Cep104 increases centriole length by promoting centriolar microtubule growth[25,28,29]. Accordingly, Cep104 overexpression may produce abnormally long centrioles that fragment, resulting in apparent centriole amplification as observed with Klp10a depletion (Figure S3F)[10]. Therefore, we overexpressed GFP-tagged Cep104 and measured centriole numbers as a readout for centriole over-elongation. Notably, Cep104-GFP overexpression produced supernumerary centrioles (Figure 3A) and increased centriole length compared to controls (Figures 3B and C). While we interpret centriole amplification to be the result of fragmentation, we do not directly test this and cannot exclude alternative causes. Interestingly, overexpression of

N-terminally tagged GFP-Cep104 did not result in centriole amplification, indicating that N-terminal tagging of Cep104 interferes with its function but not its localization (Figure 3A). We also observed an abnormal accumulation and extension of Plp on daughter centrioles, suggesting an increase in their length as well as premature Plp recruitment (Figure 3D). Additionally, wing disc cells overexpressing Cep104-GFP showed centriole elongation (Figures 3E and 3F). This contrasts with work in human cells where overexpression of Cep104 does not alter centriole length; however, the Cep104 constructs in that study were N-terminally tagged and thus potentially inactive[25].

Since Cep104 alters microtubule geometry at the tips of flagella and cilia by binding axonemal microtubules through its TOG domain, and HsCep104's TOG domain can polymerize microtubules *in vitro*[25,27–29,33,34], we tested whether a similar mechanism promotes centriole elongation. Key residues within the TOG Heat Repeats A, B, and E were mutated to negatively charged residues (F477E, A531E, V532D, and R667E; called TOGmut) to disrupt Cep104 binding to microtubules[27–29, 41]. Purified Cep104 TOGmut showed a markedly decreased ability to co-sediment with taxol-stabilized microtubules compared to WT TOG (Figure 3G). Furthermore, when Cep104-GFP was highly overexpressed in S2 cells, it decorated the interphase microtubule array in addition to centrioles (Figure 3H, left). In contrast, Cep104-TOGmut-GFP did not, and instead formed cytoplasmic puncta (Figure 3H, right). Although Cep104-TOGmut-GFP localized to centriole distal tips, it was unable to produce overly long centrioles compared to its wild-type counterpart (Figure 3I–K). Thus, our results indicate that Cep104 promotes centriole elongation by binding to, and stabilizing, the distal tips of centriolar microtubules.

Cep104 and Cep97 display independent, synergistic functions during spermiogenesis

Removal of centriole distal tip proteins is an early prerequisite step for vertebrate ciliogenesis[18]. However, a recent study of *cep97* null mutant flies found structural defects in both mechanosensory cilia and spermatid flagella, revealing an unexpected requirement for Cep97 in forming these organelles[16]. Unlike Cep97 or CP110, Cep104 redistributes to the tips of cilia (and flagella) where it regulates axonemal microtubule morphology and function[26,29,33,34]. Cep104 depletion results in shorter primary cilia in human RPE-1 cells, and mutations in Cep104 are linked to ciliopathies, such as Joubert Syndrome[29,42,43]. Because the role of *Drosophila* Cep104 in ciliogenesis was unknown when we initiated our study, we examined the effects of centriole distal tip proteins on spermatid production, a model system for the formation of flagella[44]. Although *cep104* null mutants were viable and fertile, males were less fertile than wild-type (*y,w*) flies, a trend we also observed in *cep97* mutants (Figure 4A). Strikingly, *cep104 cep97* double mutant males were nearly sterile (Figure 4A), indicating a functional synergy between these proteins which was reflected in the pronounced diminutive size of the sperm-storing seminal vesicles in double mutant males (Figures 4B and 4C)[45,46].

To determine the cause of males sterility in *cep104 cep97* double mutants, we analyzed post-meiotic spermatid development. During spermiogenesis, the 64 spermatid nuclei and their attached basal bodies share a common cyst and become aligned[44]. Single *cep104* or *cep97* null mutants each showed a small degree of misalignment of spermatid heads, but

cep104 cep97 double mutant testes exhibited almost half the expected number of aligned nuclei, with additional misplaced DNA aggregates spread throughout the length of the testes (Figures 4D, S4A, S4D, and S4E). While the origins of these DNA aggregates are unknown, mispositioned sperm may die, leaving behind aggregates that contain both nuclear and mitochondrial DNA. Additionally, the distal tips of spermatid axonemes were poorly aligned in all mutant genotypes, but most severely in *cep104 cep97* mutants where axonemes appeared tangled (Figure 4E).

We next inspected the individualization complexes (IC) that separate the sperm and ensheathes them in membrane[47]. ICs are clusters of 64 actin cones that travel together from the basal bodies along the axonemes to mediate their sperm-separating function[47,48]. Unlike the mild phenotypes seen in the individual mutants, ICs were severely disorganized in *cep104 cep97* double mutants, with actin cones facing opposite directions and separated from each other (Figures 4F and S4F). Cysts of spermatids undergoing individualization can be labelled with Cleaved Caspase 3 (CC3) and the loss of Waste Bags and Cystic Bulges (consequences of efficient sperm individualization) further support the observation that sperm individualization is perturbed in double mutants (Figures S4B, S4C and S4G)[45,48]. Taken together, our findings suggest that Cep104 and Cep97 contribute to spermiogenesis through independent, but synergistic mechanisms, to align axonemes and facilitate sperm individualization (Figure S4H).

We also measured the lengths of giant centrioles in spermatocytes (meiosis II) to determine if the *cep104 cep97* synergistic phenotypes manifest prior to spermiogenesis. In spermatocytes, centrioles are converted into basal bodies, producing short primary cilia that persist throughout division[49]. Therefore, we used Asl-staining to measure centriole length because Asl does not label axonemes. Centrioles were approximately 15% longer in both the *cep104* and *cep97* single mutants (as previously reported for a *cep97* deletion mutant)[16]. Although double mutant centrioles were no longer than in the single *cep97* mutant, centrioles were longer compared to the *cep104* mutants (Figure 4G). Given these results, it is possible that length defects incurred on basal bodies contribute to the subsequent synergistic effects of the double mutant on post-meiotic spermatid maturation. Furthermore, our findings indicate that length control is different when centrioles are associated with cilia; centrioles were longer in *cep104* null mutant spermatocytes, unlike non-ciliated S2 and wing disc cells (Figure 2). Regardless, Cep104's ability to induce centriole over-elongation may be ubiquitous. To test this, we overexpressed Cep104-GFP in the testes and measured centriole length in spermatocytes (Figure 4H). We found that centrioles were 5% longer in Cep104-GFP expressing spermatocytes (but, interestingly, not as long as in *cep104* deletion mutants). Thus, Cep104 can promote centriole elongation in cells regardless of ciliary status.

Lastly, we tested whether Cep104 might be involved in the formation or function of non-motile cilia, such as in ciliated mechanosenory neurons. Loss of mechanosensory function manifests as an uncoordinated phenotype and can be assessed using a climbing assay. We found that neither *cep104* or *cep97* null mutants showed a locomotion phenotype (Figure S5B). However, a *cep104 cep97* double mutant took more than twice the amount of time to a climb a set distance (Figure S5A), suggesting that, similar to their role in spermiogenesis, Cep104 and Cep97 act synergistically in the proper function of mechanosensory cilia.

Cep97 and Cep104 localize to distinct microtubule structures within spermatids

To identify possible explanations for the synergistic phenotypes we observed during sperm production in the *cep104 cep97* double mutant flies, we next examined the localization of Cep104 and Cep97 GFP fusion proteins expressed in testes. Interestingly, we found examples of distinct as well as overlapping localization patterns for Cep104 and Cep97. During spermatid maturation, Cep104-GFP (but not Cep97-GFP) decorated the dense complex, a microtubule-based structure associated with the basal body that lines the elongated nuclei within the spermatid head, analogous to the manchette in mammalian sperm (Figure 5A)[50–52]. Conversely, we confirmed that Cep97-GFP localized to axonemes ahead of the migrating ICs, as previously described[16], but Cep104-GFP was noticeably absent (Figure 5B). However, Cep97-GFP and Cep104-GFP co-localized in two regions: the distal tips of elongated centrioles in pre-meiotic spermatocytes, which assemble immotile cilia (Figure 5C), and the distal tips of axonemes at sperm tails (Figure 5D)[16]. Within the sperm tail, axonemes are separated from the distal membrane-compartmentalized short cilium (ciliary cap) by a gating structure called the ring centriole, identified by expression of Unc[53,54]. We found that Cep104-GFP localized proximal to the ring centriole (marked by Unc-RFP) and not within the short cilium (Figure S5B). Surprisingly, while Cep97 localized exclusively at the distal tips of pre-meiotic spermatocyte centrioles, Cep104-GFP also localized along the entire centriole (Figure 5C). (This pattern differs from a recent study showing that Cep104-GFP was restricted to centriole distal tips in spermatocytes[55]).

Since null mutations in either *cep104* or *cep97* cause disorganization of axonemes in maturing spermatids and Cep97 functions as a recruitment factor for its interacting partner CP110[16,18,36], we asked whether Cep104's localization within ciliated germline cells was dependent upon Cep97. In *cep97* null mutant flies, Cep104-GFP was no longer present on axonemal tips within spermatid tails (Figure 5E), nor was it found at the distal tips of spermatocyte centrioles (Figure 5F). However, in two regions where Cep97 is normally not found -- the dense complex and along the spermatocyte centrioles -- Cep104-GFP localization was unperturbed (Figures 5F and 5G). Altogether, our findings suggest that Cep104 and Cep97 function within distinct regions of spermatids to complete their individualization. At spermatid tails, Cep104 localization is dependent on Cep97 where they may cooperate in axoneme alignment or growth. However, within spermatids, Cep104 and Cep97 localize independently to the dense complex and IC, respectively, and likely play different roles in axoneme alignment and individualization, potentially explaining their synergistic functional relationship (Figure S4H).

Cep97 acts as a platform to recruit proteins to the distal tip of centrioles – collectively referred to as the Distal Tip Complex (DTC)

Since Cep97 recruits Cep104 to the distal tips of spermatocyte centrioles and maturing spermatid axonemes *in vivo*, we next tested whether Cep97 functions as a central scaffold for proteins that target the distal tip of centrioles in non-ciliated somatic cells. Using RNAi in S2 cells, we depleted Klp10a, Cep97 or CP110 and assessed the localization of Cep104-GFP (Figure 6A). Cep104-GFP localized to the tips of centrioles in CP110-depleted cells and overly long centrioles in Klp10a-depleted cells but was not detected on centrioles after Cep97-depletion (Figure 6A). (Although either Cep97 or CP110 RNAi resulted in

centriole loss, some centrioles were found in these cultures despite the lack of new centriole biogenesis.) Likewise, Cep104-GFP localization to centrioles in *cep97* null mutant wing disc cells was significantly decreased; although these centrioles were shorter in length, they generally maintained their structure[16] (Figures 6B and 6C). These results and the well-established observation that Cep97 recruits CP110 to centriole distal tips support the idea that Cep97 is an assembly scaffold[18,21,36].

We next tested for potential functional interactions between Cep104 and the other three distal tip proteins. Using centriole number as a readout for distal tip protein function, we found that co-depletion of Cep104 did not modify the centriole phenotypes of Klp10a, Cep97, or CP110 RNAi cells (Figures S3F and 6D). However, Cep104-GFP overexpression had an additive effect with Klp10a RNAi by significantly increasing the percentage of cells with >2 centrioles (Figure 6E), similar to overexpression of MAST/Orbit (a TOG-domain containing protein) in Klp10a-depleted spermatocytes[22]. These findings suggest that Cep104 opposes Klp10a's function in microtubule depolymerization.

Lastly, we mapped the interaction sites between centriole distal tip proteins using GFP immunoprecipitation of transgenic proteins expressed in S2 cells. Co-expression of V5-tagged Cep104 with one of ten different GFP-tagged centriole proteins (including the long or short isoform of CP110[14]) revealed that Cep104 bound only Cep97 and itself (Figure 7A, lanes 8 and 11, S6B and S6C), indicating that Cep97 is the sole centriole recruitment factor for Cep104.

The regions of Cep104 and Cep97 required for binding were identified by co-immunoprecipitation experiments in cells expressing a series of Cep104 and Cep97 truncation/deletion constructs (Figures 7B and S6A) in cells that had been depleted of the relevant endogenous proteins by UTR-targeted dsRNA (Figure S3A–C). We found that both the Cep104 N-terminal Jelly Roll (JR) and adjacent coiled coil (CC) bind Cep97 (Figure 7C). To more precisely map this interaction, we expressed a new series of C-terminal truncations in Cep104 that ended at the JR domain (Figure 7D). Our immunoprecipitations showed that, as additional Cep104 sequence was appended to the JR domain, Cep97 binding increased, reaching maximal binding with a construct containing amino acids 1–453 (Figure 7E). We believe these data demonstrate that Cep104 binds Cep97 along a large binding surface. Reciprocal experiments mapped the Cep104-binding site in Cep97 to a large central and C-terminal segment (F2 and F3; Figures S6A and S6D). Furthermore, deletion of either the Cep97-binding JR or CC domains significantly reduced GFP-Cep104's centriole distal tip localization, as demonstrated by the decrease in centrioles with two associated spots of Cep104 (Figure 7F). In summary, Cep97 recruits Cep104 to centriole distal tips through interactions involving large interfaces of their C- and N-terminal regions, respectively.

All interaction sites between Cep104, Cep97, CP110 and Klp10a were mapped by immunoprecipitation (Figures S6 and S7). Notable findings include: (1) Cep104 self-interacts through JR-JR and CC-CC binding (Figures S6E), (2) Cep97 fragment-3 (aa 514–806) binds CP110 fragment-1 (aa 1–325) (Figures S6F and S6G)[18,56], (3) CP110-F1 interacts with Klp10a N-terminus (aa 1–204) (Figures S7A–D)[10], and (4) Klp10a self-interacts through its Motor-domain and C-terminus (aa 279–805) (Figures S7E). Taken

together, our results suggest that Cep104-Cep97-CP110-Klp10a form a complex that we refer to as the Distal Tip Complex (DTC) with Cep97 acting as the foundational unit (Figure 7G). While our fly DTC interactome generally agrees with previous findings, a few key differences exist compared to their human homologs: (1) fly Cep104 JR can self-associate, (2) unlike HsCep104, fly Cep104 does not interact with CP110[27–29], and (3) Klp10a's self-interaction is not restricted to its C-terminus, as found for the human kinesin-13, MCAK[57].

DISCUSSION

Here, we describe a new component of the centriole length regulating Distal Tip Complex (DTC) in *Drosophila*, CG10137/Cep104. Cep104 is recruited to the distal tip of centrioles by Cep97, and its microtubule-binding TOG domain promotes centriole elongation. While Cep104 is required for proper centriole growth in S2 cells, it is dispensable for centriole growth in wing disc cells, highlighting the variation in centriole length control even among different somatic cell-types. Similar variation is observed with other distal tip proteins. For example, centrioles are absent in CP110-depleted S2 cells (Figure S3B and S3F)[10], but either shorter or unchanged in *cp110* mutant wing disc cells[14,16]. We propose that Cep104 is a microtubule polymerase within the DTC that promotes distal centriole growth. While Cep104 overexpression promotes centriole over-elongation in *Drosophila*, both non-ciliated (S2 and wing disc cells) and ciliated (spermatocyte) cells, Cep104 does not have this effect in human cells[25]. Possibly, additional regulatory mechanisms evolved in humans that prevent spurious growth, such as the LID domain within the PN2/3 region of CPAP/HsSas4, or the EB1-binding motif in HsCep104 that may shuttle excess Cep104 away from centrosomes – neither of which exist in DmSas4 or DmCep104[11,25]. Moreover, the tendency of some human cells to undergo ciliogenesis when the DTC is perturbed may mask the effects of HsCep104 overexpression[11,18,25]. Regardless, we also found that overexpressing Cep104 with an N-terminal tag prevented it from inducing centriole over-elongation, and previous studies with HsCep104 used N-terminal tags[25].

Our *in vivo* analyses of male *cep104* null mutant flies showed reduced fertility, longer centrioles within meiotic spermatocytes, misalignment of spermatid axonemes and defects in sperm individualization. Many of these phenotypes synergized with loss of Cep97 to produce enhanced defects during spermiogenesis, including sterility, suggesting that they either work in different pathways or function redundantly in the same pathway. Regarding the function of the sperm individualization complex (IC), it is worth noting that ICs begin near the nucleus and continue along the spermatid axoneme[47]. Previous genetic studies suggest that assembly of the IC is sensitive to nuclear shape, basal body attachment to the nucleus, and recruitment of F-actin to the dense complex[58–61]. Furthermore, synchronous movement of the IC maintains the proper orientation of actin cones during individualization[62,63]. Together, Cep97 and Cep104 knockouts result in dramatic axoneme disorganization. We propose that failure to individualize arises initially from dysregulated growth of spermatid axonemes, resulting in spatial disorganization of nuclei and ICs.

cep97 cep104 double mutants were uncoordinated, suggesting that these proteins also act synergistically for normal formation or function of mechanosensory cilia. While preparing our manuscript, *Drosophila* Cep104 was identified in an RNAi screen for genes associated

with cilium assembly or motility, and its tissue specific depletion produced an uncoordinated phenotype[55]. Further analysis revealed that distal axonemes in *cep104* mutant chordotonal neurons were shorter than controls and contained displaced microtubule doublets[55]. In contrast, *cep97* null sensory neurons contain basal bodies but frequently lack cilia[16]. While it remains unclear why the *cep97* and *cep104* single mutants used in our study show normal locomotion, the structural differences observed in sensory cilia between the individual *cep97* and *cep104* mutants may explain their functional synergy.

An outstanding question in the field is how DTC proteins collaborate to regulate centriole elongation and maintain length of mature centrioles. Centriole growth is characterized by stabilization of the microtubules that line centrioles[64–68]. In cells overexpressing microtubule-stabilizing proteins, like CPAP/Sas4, the microtubules grow asynchronously and, consequently, centriole distal ends appear distorted[4,6,11,13,14,64,65]. Although most DTC subunits are thought to either promote centriole shortening (Klp10a) or cap centrioles to prevent elongation and shortening (Cep97-CP110), the DTC is present at distal tips during times of growth. Because loss of DTC subunits results in individual microtubules extending from centriole distal tips, we propose that the DTC ensures that elongation is coordinated among the nine bundles of microtubules.

While we show that Cep104 can promote microtubule polymerization at the distal tip, we hypothesize it may possess additional functions. During periods when centriole length remains stable, Cep104 may restrict access of other microtubule polymerases to the distal tip, such as Sas4/CPAP or CLASP (MAST/Orbit)[11,70], thus enforcing centriole length stability and explaining how DTC loss leads to growth of centrioles in *Drosophila* spermatocytes. Likely, coordinated activity of the four DTC subunits with Sas4/CPAP is temporally regulated to accomplish proper length control. By characterizing Cep104 and mapping the DTC interactome, we have taken the first steps into identifying how these proteins cooperate to regulate centriole length throughout the cell cycle. However, additional studies are required to fully understand DTC regulation and how mis-regulation promotes centriole over-elongation and the resultant centriole amplification observed in cancer cells[6].

STAR METHODS

RESOURCE AVAILABILITY

Lead Contact—Further information and requests for resources and reagents should be directed to and will be fulfilled by the Lead Contact, Gregory Rogers (gcrogers@arizona.edu)

Materials Availability—Fly strains, plasmids, cell lines, and antibodies generated in this study are available upon request from the Lead Contact.

Data and Code Availability

- The published article includes all datasets generated or analyzed during this study and will be shared by the lead contact upon request.
- This paper does not report original code.

- Any additional information required to reanalyze the data reported in this paper is available from the lead contact upon request.

EXPERIMENTAL MODEL AND SUBJECT DETAILS

***Drosophila melanogaster* stocks and husbandry—**All strains used are listed in the Key Resource Table. Fly stocks were maintained on Bloomington Recipe Fly Food (LabExpress). Crosses were performed at 25°C. The following fly strains were used in this study: *y,w* (gift from Mark Peifer, University of North Carolina, Chapel Hill), *cep97*$^{\Delta 16}$, *ubi::Cep97-GFP*[56], *ubi::CP110-GFP*[53], *cep104*$^{\Delta}$ (this study), and *ubi::Cep104-GFP* (this study). Transgenic flies were generated using standard P-element transformation (Bestgene, Inc.). *cep104*$^{\Delta}$ null mutant flies were generated by CRISPR-mediated genome editing.

Cell culture—*Drosophila* S2 cells (Invitrogen) were cultured in Sf-900II SFM media (Life Technologies) as previously described[71]. dsRNA and DNA plasmids were transfected into S2 cells by nucleofection as previously described[72]. For immunoprecipitation assays, RNAi was performed for 8 days; 40 μg double-stranded (ds) RNA was transfected on day 0 and day 4 and 2 μg of DNA was transfected on Day 4, concurrent with dsRNA transfection. For immunofluorescence microscopy and preparation of whole cell lysates for Western blotting, RNAi was performed for 12 days; cells were transfected with 40 μg dsRNA on days 0, 4, and 8. 2 μg of DNA was transfected on days 4 and 8, concurrent with dsRNA transfection. For all experiments, gene expression was induced with 0.2–1 mM $CuSO_4$ on Day 5 and cells were maintained in $CuSO_4$ throughout the remainder of the experiment. Control dsRNA was generated as previously described[72]. dsRNA targeting Klp10a UTR, CP110 UTR, and Cep104 UTR were synthesized from PCR product of 3' UTR sequences of cDNAs fused to the T7 RNA polymerase promoter sequence: 5'-TAATACGACTCACTA. dsRNAs targeting Cep97 was synthesized from the PCR product of the T7 RNA polymerase promoter sequence fused to 5'–3' UTR fusion constructs in which the Cep97 coding region was deleted from the cDNA by mutagenesis. dsRNA for all Cep104 constructs was synthesized from cDNA coding region. *In vitro* dsRNA synthesis was prepared as previously described[72]. Stable Fly-FUCCI (Addgene) S2 cells were selected with 2 μg/ml neomycin G418 (Thermo Fisher Scientific).

METHODS DETAILS

Bacterial expression, protein purification, and antibody generation—Expression and purification of recombinant protein was performed as previously described[73]. Briefly, transformed BL21(DE3)pLysS (Promega Corp) grown to log phase were induced with 0.4 mM IPTG then temperature shifted from 25°C to 14°C and incubated overnight. Cells were then lysed and incubated with the appropriate resin: MBP-tagged proteins with amylose resin (New England Biolabs), GST-tagged proteins with glutathione resin (Gold Biotechnology), and His_6-tagged proteins with HisPur™ Ni-NTA resin (Thermo Fisher Scientific). Resin was washed by gravity flow, eluted, and the eluate dialyzed into PBS. For antibody production, proteins were conjugated to KLH and injected into either 2 chicken (His_6-Cep97 514–806), 3 rats (MBP-Klp10a 1–201), 2 guinea pigs (MBP-CP110 326–549), or 2 rabbits (GST-Cep104 730–941) by Pocono Rabbit Farm and Labs. Antibodies were then affinity-purified by incubating antisera with GST-tagged versions of each protein fragment

conjugated to Affi-gel 10 resin (Bio-Rad), washed in Phosphate Buffered Saline (PBS), and eluted with low 0.2 MTris-Glycine buffer, pH 2.7 into 1/5th volume of neutralizing buffer (1 M Tris, pH8). Cep97 antibodies were further absorbed against BL21(DE3)pLysS lysate conjugated to Affi-gel 10 resin and flow-through was collected.

RT-PCR—S2 cells were treated with dsRNA for 12 days. RNA was extracted according to Qiagen RNeasy Mini Kit (Qiagen, #75144) protocol and treated with RNase-Free DNase to remove any genomic contamination (Qiagen, #79254). Concentration and purity were determined using a BioDrop Duo Spectrophotometer (Biochrom, UK). RT-PCR was then performed according to the SuperScript III One-Step system protocol (Invitrogen, #12574–018). 5 ng of total RNA was used per reaction. Reverse transcription was carried out at 55C, then 40 PCR cycles were performed on the resultant cDNA using gene-specific primers with an annealing temperature of 62C. Total reactions were run on an agarose gel for analysis. Primers used: Cep104-For (5′-CTTCCCATCCTGGTCTTCGG-3′), Cep104-Rev: (5′-CTTGCGGTCCAGATCCAACT-3′), Rp49-For (5′-AT CCGCCCAGCATACAGG-3′), and Rp49-Rev (5′-CTCGTTCTCTTGAGAACGCAG-3′).

Immunoblotting—Cells were lysed in Lysis Buffer (50 mM Tris-HCl, pH 7.2, 150 mM NaCl, 0.5% Triton X-100, 1 mM DTT, and 0.1 mM PMSF), concentrations were determined by Bradford protein assay (BioRad), followed by addition of Laemmli sample buffer. Extracts were boiled for 5 min and stored at −20°C. Samples of equal total protein were resolved by SDS-PAGE, transferred onto nitrocellulose (GE Healthcare), probed with primary and secondary antibodies, and scanned on a LiCor Odyssey CLx imager (Li-Cor Biosciences). Primary antibodies used for Western blotting include rat anti-Klp10a (this study, 1:1000), guinea pig anti-CP110 (this study, 1:1000), chicken anti-Cep97 (this study, 1:1000), rabbit anti-Cep104 (this study, 1:1000), mouse anti-V5 monoclonal (Thermo Fisher Scientific, 1:3000), mouse anti-GFP monoclonal JL8 (Thermo Fisher Scientific, 1:3000), and mouse anti-α-tubulin monoclonal DM1A (Thermo Fisher Scientific, 1:3000) or 488-conjugated streptavidin. Antibodies were diluted in Western blocking buffer (5% milk in PBS, 0.1% Tween-20). Host animal specific IRDye 800CW secondary antibodies (Li-Cor Biosciences) were prepared according to the manufacturer's instructions and used at 1:3000 dilution.

Immunofluorescence microscopy

S2 cells: Cells were spread on concanavalin A-coated glass bottom plates/coverslips and fixed in ice cold methanol for 15 minutes or 10% paraformaldehyde in HL3 (5 mM HEPES, pH 7.2, 5 mM trehalose, 10 mM $NaHCO_3$, 70 mM NaCl, 5 mM KCl, 20 mM $MgCl_2$, 115 mM sucrose) + 1 mM EGTA for 12 minutes. Cells were washed with PBS, 0.1% Triton X-100 and blocked in IF blocking buffer (5% normal goat serum [NGS] in PBS, 0.1% Triton X-100) for 30 minutes at room temperature. 488-conjugated streptavidin and primary antibodies were diluted in IF blocking buffer and slides were incubated overnight at 4°C. Antibodies were used at the following dilutions: rabbit anti-Plp (1:3000)[74], rat anti-Klp10a (1:1000), guinea pig anti-CP110 (1:3000), chicken anti-Cep97 (1:5000), rabbit anti-Cep104 (1:1000), rat anti-Asl (1:1000)[75], guinea pig anti-Spd-2 (1:500)[77], or 488-conjugated streptavidin. After 3 washes with PBS, 0.1% Triton X-100, cells were

incubated at room temperature with 3.2 μM Hoechst 33342 (Thermo Fisher Scientific) and secondary antibodies diluted in IF blocking buffer for 30 minutes: anti-host animal AlexaFluor 488 (Thermo Fisher Scientific, 1:1500), anti-host animal Rhodamine Red-X (Jackson Immunoresearch, 1:1500), and anti-host animal Cy5 (Jackson Immunoresearch 1:1500). Slides were then washed 3 times with PBS, 0.1% Triton X-100 and mounted with homemade mounting medium (PBS, 90% glycerol, and 0.1 M propyl gallate) for deconvolution microscopy or Prolong Glass (Thermo Fisher Scientific) for slides for 3D-SIM. Cells were cultured with 15 uM EdU for 20 minutes immediately prior to fixation with methanol. EdU was detected with the Click-iT EdU assay by conjugating AlexaFluor 647 dye according to manufacturer's protocol (Thermo Fisher Scientific).

Testes: Testes were dissected from 1–2 day old male flies in PBS and fixed in 4% formaldehyde for 20 minutes. Fixed testes were washed and blocked in PBS, 0.5% TritonX-100 (PBST), 5% normal goat serum (NGS). Testes were then incubated in primary antibody overnight at 4°C. Primary antibodies used were as follows: anti-Asterless (1:15,000), anti-Cleaved caspase 3 (Cell Signaling Technologies, 1:100), anti-poly-glutamylated tubulin GT335 (Adipogen, 1:500). Testes were washed and then incubated in secondary antibody (1:500, Life Technologies) for 2hr at room temperature. Alexa 488-conjugated Phalloidin staining was performed concurrently with the secondary antibody (Life Technologies, 1:1000 dilution).

Wing Discs: Third instar larvae were selected, and wing discs were dissected in PBS. For Cep97 staining, wing discs were fixed in 4% formaldehyde for 10 minutes before being blocked for 1 hour in PBS, 1% Triton X-100, 5% NGS. Wing discs were then incubated in primary antibody for 90 minutes at room temperature. For all other wing disc immunofluorescence, the procedure was identical to that used for testes. Primary antibodies: Anti-Cep97 (1:500) and anti-Asterless (1:15000).

Microscopy—Deconvolution microscopy of S2 cells was performed on the DeltaVision Core system (GE Healthcare) equipped with an Olympus IX71 microscope, 100x objective (NA 1.4), and a CoolSnap HQ2 CCD camera (Photometrics). Images were acquired and processed with softWoRx v7.00 (GE Healthcare). Structured-illumination microscopy (3D-SIM) of S2 cells was performed using a Zeiss ELYRA S1 (SR-SIM) microscope using solid-state (405/488/561/642 nm) laser lines, a 63× objective (NA 1.4), 3 pattern rotations, and an EM-CCD camera (Andor iXon). Images were acquired with Zeiss ZEN Black 2.3 software followed by SIM reconstruction, channel alignment, and maximum intensity projection. Protein colocalization and centriole counts were determined manually from micrographs. S2 cell centriole length measurements were performed in Fiji (ImageJ) and statistics and graphs were prepared in GraphPad Prism 8 (GraphPad). For measurements of centriole length using Spd2 (which specifically labels the barrel of the mother centriole) as well as their companion measurements of distance between Cep97 mother-daughter spots, these were restricted to centriole pairs where the mother centriole was viewed in transverse -- determined by two lines of Spd2 in 3D-SIM images. Length of Spd2 along the centriole barrel was measured by the full width at half maximum (FWHM) intensity in Fiji (ImageJ). The lengths for Spd2 on both sides of the mother centriole barrel were then averaged.

Spinning disk confocal microscopy of tissue was performed using a Yokogawa CSU W-1 spinning disk mounted on a Nikon Ti-2 eclipse stand. The microscope was equipped with a Prime BSI CMOS camera (Photometrics). A 20x Air (N.A., Nikon) or 100x Silicone immersion (N.A 1.4, Nikon) objective was used. Microscope control was performed through the Elements software package (Nikon). *Individualization complex spread measurements* – within one field of view (133.52×133.52μm) the distance was determined between the front of the furthest forward actin cone to the tail of the most rearward actin cone.

SIM of centrioles in wing disc was conducted using an OMX4 (GE healthcare) using immersion oil RI 1.514 and a 60× 1.42 N.A. oil immersion objective (Olympus). 3D SIM z-stacks were acquired with 0.125 μm increments and raw images were reconstructed using Softworx (Cytiva) using a wiener filter constant of 0.002–0.003. For centriole length measurements, images were cropped and subject to a 0.8 Gaussian filter. A line 5 px wide was then drawn through the center of the centriole and a line profile was plotted in ImageJ. Distance between the peaks and shoulders were then measured from the resulting plot. Shoulders were defined as half the maximum intensity of Cep97. For measurements of centriolar Cep104-GFP intensity, on a circular region of interest was drawn in the center of the Asterless (centriole) ring. The mean fluorescence intensity of that ROI was measured to determine Cep104-GFP levels.

For centriole imaging in spermatocytes, lattice SIM was performed using an Elyra7 (Zeiss) using immersion oil RI 1.518 (30°C) and a 63× 1.4 N.A. oil immersion objective (Zeiss). Lattice SIM z-stacks were acquired with 0.110 μm increments with 15 phases taken per z slice, raw images were reconstructed using Zen Black (Zeiss) using the Sim^2 mode. Centriole images were cropped. A line approximately 300 nm wide was then drawn through the center of the centriole and a line profile was plotted in ImageJ. Length of the centriole as determined by the Asterless signal was then measured from the resulting plot.

BioID proximity labeling assay—Cells were transfected with the highly active biotin-ligase V5-tagged miniTurbo (containing a nuclear export signal [NES]) or V5-Cep97-miniTurbo and induced for 24 hours prior to overnight treatment with 50 μM D-Biotin (Figure S1A). Western blotting was performed as described above, however, blots were washed with TBS-T (50 mM Tris pH 7.4, 125 mM NaCl, 0.1% Tween-20) and Streptavidin-800CW was diluted 1:1000 in TBS-T, 3% Milk, 0.02% SDS (Figure S1B). As previously published[23], cells were then lysed in BioID lysis buffer (50 mM Tris-HCl, pH 7.2, 500 mM NaCl, 0.5% Triton X-100, 1 mM EDTA) and excess biotin was removed with a polyacrylamide desalting column. Protein containing fraction were then mixed with 200 ul streptavidin-coated Dynabeads and incubated at 4°C overnight. Beads were then washed with Wash 1 (BioID lysis buffer, 0.5% Triton X-100, 0.1% deoxycholic acid) and then Wash 2 (50 mM Tris-HCl, pH7.2, 250 mM LiCl, 1 mM EDTA, 0.5% deoxycholic acid, 0.5% NP-40). Beads were extensively washed in 50 mM NH_4HCO_3 and resuspended in 100 ul of 10 mM NH_4HCO_3.

Recovered product was then subjected to tandem mass spectrometry (MS/MS) to identify proteins (Figure S1C; Data S1). Normalized spectral abundance factors (NSAF) were analyzed as previously published on proteins with at least 2 unique peptides identified[76].

Enrichment in the V5-Cep97-miniTurbo sample was determined by normalizing to NSAF counts from V5-miniTurbo-NES and enriched proteins were identified as having a score > 1. MS/MS data we generated by the Taplin Mass Spectrometry Facility (Harvard Medical School) and deposited in the UCSD MassIVE Repsitory (MSV000092404).

DNA Constructs—To generate S2 cell expression constructs, full-length cDNAs Cep97 (DGC EST library 1.0), CP110 (DGRC, RE58503), Klp10a (DGC EST library 1.0), and Cep104 (DGC EST library 1.0) were PCR amplified (Phusion polymerase, Thermo Fisher Scientific) and subcloned into the pMT/V5-HisC vector containing in-frame coding sequences for EGFP or V5 under the control of a metallothionein-inducible promoter. PCR-based site-directed mutagenesis was used to make deletion mutants. To generate bacterial expression constructs, fragments of full-length cDNAs were PCR amplified and subcloned in-frame into pMal-c2x (MBP-tagged constructs), pGEX-6p2 (GST-tagged constructs), or pET28a (His_6-tagged constructs).

CRISPR/Cas9 editing: To generate the CRISPR deletion of Cep104 two guide RNAs (gRNA) and one homology donor construct were injected into embryos expressing Cas9 under control of the vasa promoter. gRNAs were cloned into the pU6:Bbs1-ChiRNA vector[79] using the following primers: Cep104 5'F: CTTCGTTGGACCGACACTACTGGA 5'R: AAACTCCAGTAGTGTC GGTCCAAC, 3'F: CTTCGAGGCGAACACCACGTTAA, 3' R: AAACTTTAACGTGGTGTT CGCCTC. Homology arms were cloned using Gibson assembly into a vector backbone on either side of 3xP3 RFP which expresses RFP in the eyes to facilitate screening for genome integration. The following primers were used: 5' Fwd: GTACTTCGCGAATGCGTCGAGATACCAATGCAGTACATCCTTCTTGTAGAGCCTGA AGGA, 5' Rev: CGCTTCTGACCTGGGAAAACGT GAAGAATTGTTGACGTCGCGCCGTCAAAAGCGCACTAC, 3' Fwd: CGTATAATGTATG CTATACGAAGTTATAGGAAAGCGTACACTTAATC GATCTATTGGCCT, 3' Reverse: CTCGTCGGTCCCGGCATCCGATCCAATAGGAAAACA CGCGACGGTCTTCAAAAAGG AGAG. Injected males were crossed with *y,w* females in order to remove the Vasa-Cas9. The offspring of this cross were screened for males expressing RFP in the eyes. These males were then crossed once more to a balancer stock. The deletion was confirmed by PCR (Figure 2F) using the following primers: Cep104 Screening Forward: TTGGAACACGTAGCCTTTGGACAC and Reverse: TACTGGTGGTTCATCAAGCGTCTG.

cep97$^{\Delta}$ *cep104*$^{\Delta}$ double mutants were generated by genetic recombination. Flies were screened for the presence of both deletions using the following primers: Cep97 Fwd: CGCCTCCAATTATCGATAGACGTA, Cep97 Reverse: CTGTTTGGGTTAACAAAGCACAGT; expected size: 680bp. Cep104 Fwd: AGAGAGTCGTAATCGTTGTCTGGG, Cep104 Rev: AACTGACGCGAATAGAACTGCTCC; expected size: 916bp. Cnn Fwd: TGTTAGGTTTTTCGAGGGG, Cnn Rev: TCGTCTATGCTTTTGGACAG; expected size: 651bp.

Immunoprecipitation—Immunoprecipitation (IP) assays were performed as previously described[77]. Recombinant, purified GFP-Binding Protein (GBP) fused to human Fc domain was bound to magnetic Protein A Dynabeads (ThermoFisher), and then cross-linked with dimethyl pimelimidate[72]. GBP-coupled Dynabeads were stored in PBS, 0.1% Tween 20 at 4°C. Prior to use, beads were equilibrated in IP buffer (50 mM Tris, pH 7.2, 125 mM NaCl, 1 mM EGTA, 1 mM DTT, 0.5% Triton X-100, 1x SigmaFast Protease inhibitors, 0.1 mM PMSF, and 1 μg/ml soybean trypsin inhibitor). Transfected cells were harvested, lysed in IP buffer, lysate concentration was determined by Bradford assay, and lysates were diluted to 5 mg/ml. Lysates were then clarified by centrifugation at 10,000 × g for 5 minutes at 4°C and inputs were made from pre-cleared lysates in Laemmli Buffer. GBP-coated beads were rocked with lysates for 30 minutes at 4°C, washed four times by resuspending beads in 1 ml IP buffer, transferred to a new tube during the final wash, then boiled in 2x Laemmli sample buffer.

Microtubule Co-sedimentation—Microtubule co-sedimentation assays were performed as previously described[78]. Briefly, 10 μM porcine tubulin heterodimers were polymerized at 37°C in BRB80 buffer (80 mM PIPES, pH 6.8, 1 mM $MgCl_2$, and 1 mM EGTA) containing 1 mM GTP and 1 mM DTT using increasing concentrations of paclitaxel (final concentration 20 μM). Purified His_6-TOG domain and TOGmutant (TOGmut) were exchanged into BRB80, 100 mM KCl, 1 mM GTP, 1 mM DTT, and 20 μM paclitaxel, then incubated with varying concentrations of microtubules (final 50 mM KCl) for 20 minutes and sedimented for 30 minutes at 70,000 × g, 25°C. Supernatant was removed and microtubule pellets were resuspended in a volume of 2x Laemmli sample buffer equal to the supernatant volume. Equal volumes of supernatant and pellet were resolved on Coomassie-stained SDS-PAGE. Densitometry was performed on protein gels using Fiji (ImageJ) and relative TOG bound to microtubules was calculated in Microsoft Excel. Best-fits were performed in Prism 9 (GraphPad).

Male fertility assay—Virgin *y,w* females and males of the experimental genotype were incubated at 25°C for three days. Males were then individually added to vials containing 5 females and mated for 90 minutes. Males were removed and the females were allowed to lay eggs for 24 hours. Offspring were counted prior to eclosion from the pupal case.

Climbing assay—Climbing/bang assay was performed using a modified version described in Dobbelaere et al., (2020)[16]. 10 three-day-old adult males of each genotype were collected in 14 cm tubes. Flies were allowed to recover from the CO_2 and left in the tube for 20 min to recover. Flies were then banged to the bottom of the tube and recorded climbing back upward. The time measured represents the point at which 5 flies (half) had climbed above the 7 cm (halfway) point. Each data point represents an independent experiment of 10 male flies.

Quantification and Statistical Analysis—The following statistical test were performed: 2-way AVOVA analysis with Tukey's t-test (Figures 2B, 3A, and S3F), two-tailed, unpaired t-test (Figures 2D, 2E, 2G–I, 2L, 2M, 3B, 3C, 3E, 3F, and 4H), ordinary

one-way ANOVA with Tukey's t-test (Figures 3J, 3K, 4A, 4G, S5A, S6B, and S6C), and one-way ANOVA with Dunnett's multiple comparison (Figures 4C, S4D–G).

Supplementary Material

Refer to Web version on PubMed Central for supplementary material.

ACKNOWLEDGEMENTS

We thank Drs. Daniel Buster for critical review of the manuscript, Renata Basto for the anti-Spd2 antibody, and Kevin Slep for designing TOGmut. N.M.R thanks the Division of Intramural Research at the National Institutes of Health/National Heart, Lung, and Blood Institute (1ZIAHL006126) for their support. G.C.R is grateful for support from National Institute of General Medical Sciences R35GM136265 as well as the National Cancer Institute P30CA23074.

REFERENCES

1. Vasquez-Limeta A, and Loncarek J (2021). Human centrosome organization and function in interphase and mitosis. Semin. Cell Dev. Bio 117, 30–41. 10.1016/j.semcdb.2021.03.020. [PubMed: 33836946]
2. Bornens M (2021). Centrosome organization and functions. Curr. Opin. Struct. Bio 66, 199–206. 10.1016/j.sbi.2020.11.002. [PubMed: 33338884]
3. Gonzalez C, Tavosanis G, and Mollinari C (1998). Centrosomes and microtubule organization during Drosophila development. J. Cell Sci 111, 2697–2706. 10.1242/jcs.111.18.2697. [PubMed: 9718363]
4. Kohlmaier G, Loncarek J, Meng X, McEwen BF, Mogensen MM, Spektor A, Dynlacht BD, Khodjakov A, and Gönczy P (2009). Overly long centrioles and defective cell division upon excess of the Sas-4-related protein CPAP. Curr. Biology 19, 1012–1018. 10.1016/j.cub.2009.05.018.
5. Lin Y-N, Wu C-T, Lin Y-C, Hsu W-B, Tang C-JC, Chang C-W, and Tang TK (2013) CEP120 interacts with CPAP and positively regulates centriole elongation. J. Cell Bio 202, 211–219. 10.1083/jcb.201212060. [PubMed: 23857771]
6. Marteil G, Guerrero A, Vieira AF, de Almeida BP, Machado P, Mendonça S, Mesquita M, Villarreal B, Fonseca I, Francia ME, et al. (2018). Over-elongation of centrioles in cancer promotes centriole amplification and chromosome missegregation. Nat. Commun 9, 1258. 10.1038/s41467-018-03641-x. [PubMed: 29593297]
7. Carvalho-Santos Z, Machado P, Branco P, Tavares-Cadete F, Rodrigues-Martins A, Pereira-Leal JB, and Bettencourt-Dias M (2010). Stepwise evolution of the centriole-assembly pathway. J. Cell Sci 123, 1414–1426. 10.1242/jcs.064931. [PubMed: 20392737]
8. Sharma A, Olieric N, and Steinmetz MO (2021) Centriole length control. Curr. Opin. Struct. Bio 66, 89–95. 10.1016/j.sbi.2020.10.011. [PubMed: 33220554]
9. Chrétien D, Buendia B, Fuller SD, and Karsenti E (1997). Reconstruction of the centrosome cycle from cryoelectron micrographs. J. Struct. Bio 120, 117–133. 10.1006/jsbi.1997.3928. [PubMed: 9417977]
10. Delgehyr N, Rangone H, Fu J, Mao G, Tom B, Riparbelli MG, Callaine G, and Glover DM (2012). Klp10A, a microtubule-depolymerizing kinesin-13, cooperates with CP110 to control Drosophila centriole length. Curr. Biology 22, 502–509. 10.1016/j.cub.2012.01.046.
11. Sharma A, Aher A, Dynes NJ, Frey D, Katrukha EA, Jaussi R, Grigoriev I, Croisier M, Kammerer RA, Akhmanova A, et al. (2016). Centriolar CPAP/SAS-4 imparts slow processive microtubule growth. Dev. Cell 37, 362–376. 10.1016/j.devcel.2016.04.024. [PubMed: 27219064]
12. Zheng X, Ramani A, Soni K, Gottardo M, Zheng S, Gooi LM, Li W, Feng S, Mariappan A, Wason A, et al. (2016). Molecular basis for CPAP-tubulin interaction in controlling centriolar and ciliary length. Nat. Commun 7, 11874. 10.1038/ncomms11874. [PubMed: 27306797]

13. Schmidt TI, Kleylein-Sohn J, Westendorf J, Le Clech M, Lavoie SB, Stierhoff Y-D, and Nigg EA (2009). Control of centriole length by CPAP and CP110. Curr. Biology 19, 1005–1011. 10.1016/j.cub.2009.05.016.
14. Franz A, Roque H, Saurya S, Dobbelaere J, and Raff JW (2013). CP110 exhibits novel regulatory activities during centriole assembly in Drosophila. J. Cell Bio 203, 785–799. 10.1083/jcb.201305109. [PubMed: 24297749]
15. Gottardo M, Callaini G, and Riparbelli MG (2016). Klp10A modulates the localization of centriole-associated proteins during Drosophila male gametogenesis. Cell Cycle 15, 3432–3441. 10.1080/15384101.2016.1248005. [PubMed: 27764551]
16. Dobbelaere J, Schmidt Cernohorska M, Huranova M, Slade D, and Dammermann A (2020). Cep97 is required for centriole structural integrity and cilia formation in Drosophila. Curr. Biology 30, 3045–3056.e7. 10.1016/j.cub.2020.05.078.
17. Kobayashi T, Tsang WY, Li J, Lane W, and Dynlacht BD (2011). Centriolar kinesin Kif24 interacts with CP110 to remodel microtubules and regulate ciliogenesis. Cell 145, 914–925. 10.1016/j.cell.2011.04.028. [PubMed: 21620453]
18. Spektor A, Tsang WY, Khoo D, and Dynlacht BD (2007). Cep97 and CP110 suppress a cilia assembly program. Cell 130, 678–690. 10.1016/j.cell.2007.06.027. [PubMed: 17719545]
19. Tsang WY, Bossard C, Khanna H, Peranen J, Swaroop A, Malhotra V, and Dynlacht BD (2008). CP110 suppresses primary cilia formation through its interaction with CEP290, a protein deficient in human ciliary disease. Dev. Cell 15, 187–197. 10.1016/j.devcel.2008.07.004. [PubMed: 18694559]
20. Reiter JF, and Leroux MR (2017). Genes and molecular pathways underpinning ciliopathies. Nat. Rev. Mol. Cell Bio 18, 533–547. 10.1038/nrm.2017.60. [PubMed: 28698599]
21. Huang N, Zhang D, Li F, Chai P, Wang S, Teng J, and Chen J (2018). M-phase phosphoprotein 9 regulates ciliogenesis by modulating CP110-Cep97 complex localization at the mother centriole. Nat. Commun 9, 4511 10.1038/s41467-017-06990-9. [PubMed: 30375385]
22. Shoda T, Yamazoe K, Tanaka Y, Asano Y and Inoue YH (2021). Orbit/CLASP determines centriole length by antagonizing Klp10A in Drosophila spermatocytes. J. Cell. Sci 134, jcs251231. 10.1242/jcs.251231.
23. Roux KJ, Kim DI, Raida M, and Burke B (2012). A promiscuous biotin ligase fusion protein identifies proximal and interacting proteins in mammalian cells. J. Cell Bio 196, 801–810. 10.1083/jcb.201112098. [PubMed: 22412018]
24. Branson TC, Bosch JA, Sanchez AD, Udeshi ND, Svinkina T, Carr SA, Feldman JL, Perrimon N, and Ting AY (2018). Efficient proximity labeling in living cells and organisms with TurboID. Nat. Biotechnology 36, 880–887. 10.1038/nbt.4201.
25. Jiang K, Toedt G, Susana MG, Davey NE, Hua S, van der Vaart B, Grigoriev I, Larsen J, Pedersen LB, Bezstarosti K, et al. (2012). A proteome-wide screen for mammalian SxIP motif-containing microtubule plus-end tracking proteins. Curr. Biology 22, 1800–1807. 10.1016/j.cub.2012.07.047.
26. Frikstad K-AM, Molinari E, Thoresen M, Ramsbottom SA, Hughes F, Letteboer SJF, Gilani S, Schink KO, Stokke T, Geimer S, et al. (2019). A CEP104-CSPP1 complex is required for formation of primary cilia competent in Hedgehog signaling. Cell Reports 28, 1907–1922.e6. 10.1016/j.celrep.2019.07.025. [PubMed: 31412255]
27. Rezabkova L, Kraatz SHW, Akhmanova A, Steinmetz MO, and Kammerer RA (2016). Biophysical and structural characterization of the centriolar protein Cep104 interaction network. J. Bio. Chem 291, 18496–18504. 10.1074/jbc.m116.739771. [PubMed: 27402853]
28. Al-Jassar C, Andreeva A, Barnabas DD, McLaughlin SH, Johnson CM, Yu M and Van Breugel M (2017). The ciliopathy-associated Cep104 protein interacts with tubulin and Nek1 kinase. Structure 25, 146–156 10.1016/j.str.2016.11.014. [PubMed: 28017521]
29. Yamazoe T, Nagai T, Umeda S, Sugaya Y, and Mizuno K (2020). Roles of TOG and jelly-roll domains of centrosomal protein CEP104 in its functions in cilium elongation and Hedgehog signaling. J. Bio. Chem 295, 14723–14736. 10.1074/jbc.RA120.013334. [PubMed: 32820051]
30. Mimori-Kiyosue Y, Shiina N, and Tsukita S (2000). The dynamic behavior of the APC-binding protein EB1 on the distal ends of microtubules. Curr. Biology 10, 865–868. 10.1016/S0960-9822(00)00600-X.

31. Jakobsen L, Vanselow K, Skogs M, Toyoda Y, Lundberg E, Poser I, Falkenby LG, Bennetzen M, Westendorf J, Nigg EA, et al. (2011). Novel asymmetrically localizing components of human centrosomes identified by complementary proteomics methods. EMBO J. 30, 1520–1535. 10.1038/emboj.2011.63. [PubMed: 21399614]
32. Gupta GD, Coyaud É, Gonçalves J, Mojarad BA, Liu Y, Wu Q, Gheiratmand L, Comartin D, Tkach JM, Cheung SWT, et al. (2015). A dynamic protein interaction landscape of the human centrosome-cilium interface. Cell 163, 1484–1499. 10.1016/j.cell.2015.10.065. [PubMed: 26638075]
33. Satish Tammana TV, Tammana D, Diener DR, and Rosenbaub J (2013). Centrosomal protein CEP104 (Chlamydomonas FAP256) moves to the ciliary tip during ciliary assembly. J. Cell Sci 126, 5018–5029. 10.1242/jcb.133439. [PubMed: 23970417]
34. Louka P, Vasudevan KK, Guha M, Joachimiak E, Wloga D, Tomasi RFX, Baroud CN, Dupuis-Williams P, Galati DF, Pearson CG, et al. (2018). Proteins that control the geometry of microtubules at the ends of cilia. J. Cell Bio 217, 4298–4313. 10.1083/jcb201804141. [PubMed: 30217954]
35. Kleylein-Sohn J, Westendorf J, Le Clech M, Habedanck R, Stierhof Y-D, and Nigg EA (2007). Plk4-induced centriole biogenesis in human cells. Dev. Cell 13, 190–202. 10.1016/j.devcel.2007.07.002. [PubMed: 17681131]
36. Aydogan MG, Hankins LE, Steinacker TL, Mofatteh M, Saurya S, Wainman A, Wong S-S, Lu X, Zhou FY, and Raff JW (2022). Centriole distal-end proteins CP110 and Cep97 influence centriole cartwheel growth at the proximal end. J. Cell Sci 135, jcs260015. 10.1242/jcs.260015.
37. Zielke N, Korzelius J, van Straaten M, Bender K, Schuhknecht GFP, Dutta D, Xiang J, and Edgar BA (2014). Fly-FUCCI: a versatile tool for studying cell proliferation in complex tissues. Cell Reports 7, 588–598. 10.1016/j.celrep.2014.03.020. [PubMed: 24726363]
38. Chen Z, Indjeian VB, McManus M, Wang L, and Dynlacht BD (2002). CP110, a cell cycle-dependent CDK substrate, regulates centrosome duplication in human cells. Dev. Cell 3, 339–350. 10.1016/s1534-5807(02)00258-7. [PubMed: 12361598]
39. D'Angiolella V, Donato V, Vijayakumar S, Saraf A, Florens L, Washburn MP, Dynlacht B, and Pagano M (2010). $SCF^{Cyclin\ F}$ controls centrosome homeostasis and mitotic fidelity through CP110 degradation. Nature 466, 138–142. 10.1038/nature09140. [PubMed: 20596027]
40. Li J, D'Angiolella V, Seeley ES, Kim S, Kobayashi T, Fu W, Campos EI, Pagano M, and Dynlacht BD (2013). USP33 regulates centrosome biogenesis via deubiquitination of the centriolar protein CP110. Nature 495, 255–259. 10.1038/nature11941. [PubMed: 23486064]
41. Ayaz P, Ye X, Huddleston P, Brautigam CA, and Rice LM (2012) A TOG:αβ-tubulin complex structure reveals conformation-based mechanisms for a microtubule polymerase. Science 337, 857–860. 10.1126/science.1221698. [PubMed: 22904013]
42. Srour M, Hamdan FF, McKnight D, Davis E, Mandel H, Schwartzentruber J, Martin B, Patry L, Nassif C, Dionne-Laporte A, et al. (2015). Joubert syndrome in French Canadians and identification of mutations in CEP104. Am. J. Hum. Genet 97, 744–753. 10.1016/j.ajhg.2015.09.009. [PubMed: 26477546]
43. Luo M, Cao L, Cao Z, Ma S, Shen Y, Yang D, Lu C, Lin Z, Liu Z, Yu Y, et al. (2019). Whole exome sequencing reveals novel CEP104 mutations in a Chinese patient with Joubert syndrome. Mol. Genet. Genomic Med 7, e1004. 10.1002/mgg3.1004. [PubMed: 31625690]
44. Fabian L, and Brill JA (2012). Drosophila spermiogenesis: big things come from little packages. Spermatogenesis, 2, 197–212. 10.4161/spmg.21798. [PubMed: 23087837]
45. Yuan X, Zheng H, Su Y, Guo P, Zhang X, Zhao Q, Ge W, Li C, Xi Y, and Yang X (2019). Drosophila Pif1A is essential for spermatogenesis and is the homolog of human CCDC157, a gene associated with idiopathic NOA. Cell Death Dis, 10, 125. 10.1038/s41419-019-1398-3. [PubMed: 30741974]
46. McCullough EL, Whittington E, Singh A, Pitnick S, Wolfner MF, and Dorus S (2022). The life history of *Drosophila* sperm involves molecular continuity between male and female reproductive tracts. Proc Natl Acad Sci U S A, 119, e2119899119. 10.1073/pnas.2119899119. [PubMed: 35254899]

47. Steinhauer J (2015). Separating from the pack: molecular mechanisms of *Drosophila* spermatid individualization. Spermatogenesis 5, e1041345. 10.1080/21565562.2015.104135. [PubMed: 26413413]
48. Huh JR, Vernooy SY, Yu H, Yan N, Shi Y, Guo M, Hay BA (2004). Multiple apoptotic caspase cascades are required in nonapoptotic roles for Drosophila spermatid individualization. PLoS Bio. 2, E15. 10.1371/journal.pbio.0020015. [PubMed: 14737191]
49. Riparbelli MG, Callaini G, and Megraw TL (2012). Assembly and persistence of primary cilia in dividing Drosophila spermatocytes. Dev. Cell 23, 425–432. 10.1016/j.devcel.2012.05.024. [PubMed: 22898783]
50. Lehti MS, and Sironen A (2016). Formation and function of the manchette and flagellum during spermatogenesis. Reproduction 151, R43–R54. 10.1530/REP-15-0310. [PubMed: 26792866]
51. Augiere C, Lapart J-A, Duteyrat J-L, Cortier E, Maire C, Thomas J, and Durand B (2019). Salto/CG13164 is required for sperm head morphogenesis in Drosophila. Mol. Bio. Cell 30, 636–645. 10.1091/mbc.E18-07-0429. [PubMed: 30601696]
52. Riparbelli MG, Persico V, and Callaini G (2020). The microtubule cytoskeleton during the early *Drosophila* spermiogenesis. Cells 9, 2684. 10.3390/cells9122684. [PubMed: 33327573]
53. Basiri M, Ha A, Chadha A, Clark NM, Polyanovsky A, Cook B, and Avidor-Reiss T (2014) A migrating ciliary gate compartmentalizes the site of axoneme assembly in Drosophila spermatids. Curr. Biol 24, 2622–2631. 10.1016/j.cub.2014.09.047. [PubMed: 25447994]
54. Vielillard J, Raschaki M, Duteyrat JL, Augière C, Cortier E, Lapart JA, Thomas J, and Durand B (2016) Transition zone assembly and its contribution to axoneme formation in Drosophila male germ cells. J Cell Biol. 214, 875–889. 10.1083/jcb.201603086. [PubMed: 27646273]
55. Dobbelaere J, Su TY, Erdi B, Schleiffer A, and Dammermann A (2023) A phylogenetic profiling approach identifies novel ciliogenesis genes in Drosophila and C. elegans. EMBO J. e113616. 10.15252/embj.2023113616. [PubMed: 37317646]
56. Galletta BJ, Fagerstrom CJ, Schoborg TA, McLamarrah TA, Ryniawec JM, Buster DW, Slep KC, Rogers GC, and Rusan NM (2016). A centrosome interactome provides insight into organelle assembly and reveals a non-duplication role for Plk4. Nat. Commun 7, 12476. 10.1038/ncomms12476. [PubMed: 27558293]
57. Hertzer KM, Ems-McClung SC, Kline-Smith SL, Lipkin TG, Gilbert SP, and Walczak CE (2006) Mol. Biol. Cell 17, 700–710. 10.1091/mbc.e05-08-0821. [PubMed: 16291860]
58. Lenz-Bohme B, Wismar J, Fuchs S, Reifegerste R, Buchner E, Betz H, and Schmitt B (1997). Insertional mutation of the Drosophila nuclear lamin Dm0 gene results in defective nuclear envelopes, clustering of nuclear pore complexes, and accumulation of annulate lamellae. J. Cell Bio 137, 1001–1016. 10.1083/jcb.137.5.1001. [PubMed: 9166402]
59. Fabrizio JJ, Hime G, Lemmon SK, and Bazinet C (1998) Genetic dissection of sperm individualization in *Drosophila melanogaster*. Development 125, 1833–1843. 10.1242/dev.125.10.1833. [PubMed: 9550716]
60. Texada MJ, Simonette RA, Johnson CB, Deery WJ, Beckingham KM (2008). *yuri gagarin* is required for actin, tubulin and basal body functions in *Drosophila* spermatogenesis. J. Cell Sci 121, 1926–1936. 10.1242/jcs.026559. [PubMed: 18477609]
61. Galletta BJ, Jacobs KC, Fagerstrom CJ, and Rusan NM (2016). Asterless is required for centriole length control and sperm development. J. Cell Bio 213, 435–450. 10.1083/jcb.201501120. [PubMed: 27185836]
62. Riparbelli MG and Callaini G (2007). The *Drosophila parkin* homologue is required for normal mitochondrial dynamics during spermiogenesis. Dev. Bio 303, 108–120. 10.1016/j.ydbio.2006.10.038. [PubMed: 17123504]
63. Vedelek V Kovacs AL, Juhasz G, Alzyoud E, and Sinka R (2021). The tumor suppressor archipelago E3 ligase is required for spermatid differentiation in Drosophila testes. Sci. Reports 11, 8422. 10.1038/s41598-021-87656-3.
64. Tang C-JC, Fu R-H, Wu K-S, Hsu W-B, and Tang TK (2009). CPAP is a cell cycle-regulated protein that controls centriole length. Nat. Cell Bio 11, 825–831. 10.1038/ncb1889. [PubMed: 19503075]

65. Gudi R, Zho C, Li J, and Gao Q (2011). Centrobin-tubulin interaction is required for centriole elongation and stability. J. Cell Bio 193, 711–725. 10.1072/jcb.201006135. [PubMed: 21576394]
66. Sydor AM, Coyaud E, Rovelli C, Laurent E, Liu H, Raught B, and Mennella V (2018). PPP1R35 is a novel centrosomal protein that regulates centriole length in concert with the microcephaly protein RTTN. Elife 7, e37846. 10.7554/eLife.37846. [PubMed: 30168418]
67. Comartin DG, Fussner E, Coyaud E, Hasegan M, Archinti MS, Pincev D, Lawo S, Raught B, Bazett-Jones DP, Lüders J, et al. (2013). CEP120 and SPICE1 cooperate with CPAP in centriole elongation. Curr. Biology 23, 1360–1366. 10–1016/j.cub.2013.06.002.
68. Vasquez-Limeta A, Lukasik K, Kong D, Sullenberger C, Luvsanjav D, Sahabandu N, Chari R, and Loncarek J (2022). CPAP insufficiency leads to incomplete centrioles that duplicate but fragment. J. Cell Bio 221, e202108018. 10.1083/jcb.202108018.
69. Mennella V, Rogers GC, Rogers SL, Buster DW, Vale RD, and Sharp DJ (2005). Functionally distinct kinesin-13 family members cooperate to regulate microtubule dynamics during interphase. Nat. Cell Bio 7, 235–245. 10.1038/ncb1222. [PubMed: 15723056]
70. Moriwaki T, and Goshima G (2016) Five factors can reconstitute all three phases of microtubule polymerization dynamics. J. Cell Biol 215, 357–368. 10.1083/jcb.201604118. [PubMed: 27799364]
71. Rogers SL, and Rogers GC (2008). Culture of Drosophila S2 cells and their use for RNAi-mediated loss-of-function studies and immunofluorescence microscopy. Nat. Protocols 3, 606–611. 10.1038/nprot.2008.18. [PubMed: 18388942]
72. McLamarrah TA, Buster DW, Galletta BJ, Boese CJ, Ryniawec JM, Hollingsworth NA, Byrnes AE, Brownlee CW, Slep KC, Rusan NM, et al. (2018). An ordered pattern of Ana2 phosphorylation by Plk4 is required for centriole assembly. J. Cell Bio 217, 1217–1231. 10.1083/jcb.201605106. [PubMed: 29496738]
73. McLamarrah TA, Speed SK, Ryniawec JM, Buster DW, Fagerstrom CJ, Galletta BJ, Rusan NM, and Rogers GC (2020) A molecular mechanism for the procentriole recruitment of Ana2. J. Cell Bio 219, e201905172. 10.1083/jcb.201905172. [PubMed: 31841145]
74. Rogers GC, Rusan NM, Roberts DM, Peifer M, and Rogers SL (2009). The SCF Slimb ubiquitin ligase regulates Plk4/Sak levels to block centriole reduplication. J. Cell. Bio 184, 225–239. 10.1083/jcb.200808049. [PubMed: 19171756]
75. Boese CJ, Nye J, Buster DW, McLamarrah TA, Byrnes AE, Slep KC, Rusan NM, and Rogers GC (2018). Asterless is a Polo-like kinase 4 substrate that both activates and inhibits kinase activity depending on its phosphorylation state. Mol. Bio. Cell 29, 2874–2886. 10.1091/mbc.E18-07-0445. [PubMed: 30256714]
76. Zybailov B Moseley AL, Sardiu ME, Coleman MK, Florens L, and Washburn MP (2006). Statistical analysis of membrane proteome expression changes in Saccharomyces cerevisiae. J. Proteome Res 5, 2339–2347. 10.1021/pr060161n. [PubMed: 16944946]
77. Gambarotto D, Pennetier C, Ryniawec JM, Buster DW, Gogendeau D, Goupil A, Nano M, Simon A, Blanc D, Racine V, et al. (2019). Plk4 regulates centriole asymmetry and spindle orientation in neural stem cells. Dev. Cell 50, 11–24.e10. 10.1016/j.devcel.2019.04.036. [PubMed: 31130353]
78. Byrnes AE, and Slep KC (2017). TOG-tubulin binding specificity promotes microtubule dynamics and mitotic spindle formation. J. Cell Bio 216, 1641–1657. 10.1083/jcb.201610090. [PubMed: 28512144]
79. Gratz SJ, Cummings AM, Nguyen JN, Hamm DC, Donohue LK, Harrison MM, Wildonger J, O'Connor-Giles KM, 2013. Genome Engineering of Drosophila with the CRISPR RNA-Guided Cas9 Nuclease. Genetics 194, 1029–1035. 10.1534/genetics.113.152710 [PubMed: 23709638]

Hightlights

- Cep104 regulates centriole growth in *Drosophila*.
- Cep104 promotes elongation by binding to centriole microtubules.
- Cep97 is a scaffold that recruits centriole “distal tip complex” proteins.
- Cep104 and Cep97 have cooperative and distinct roles during spermiogenesis.

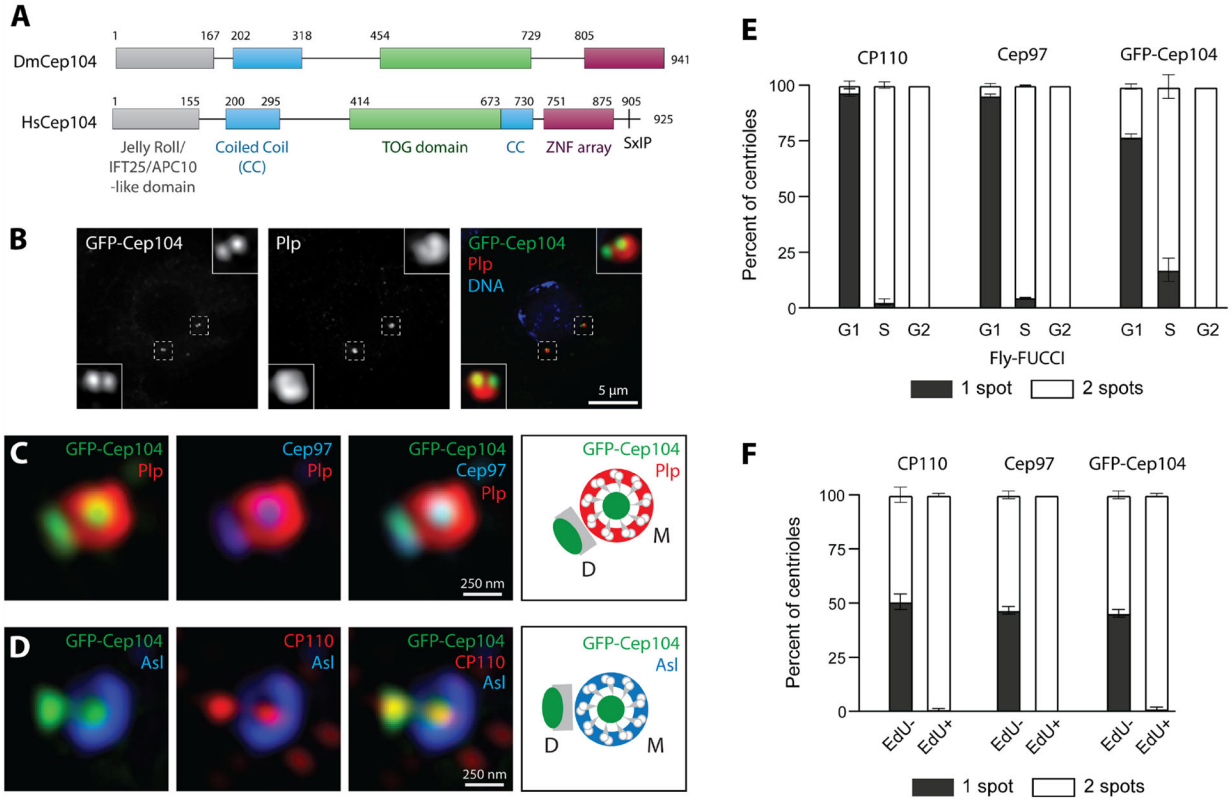

Figure 1. *Drosophila* Cep104 is recruited to the distal tip of centrioles at the G1/S-phases transition

(A) Linear maps of *Drosophila* (Dm) and human (Hs) Cep104 depicting functional and structural domains. Note the C-terminal EB1-binding domain in HsCep04 is absent in the fly homolog.

(B-D) Interphase centrioles in transgenic GFP-Cep104 (green) expressing S2 cells were imaged with conventional fluorescence microscopy (B) or 3D-SIM (C and D). Fixed cells were immunostained for Plp (red, B and C), Asl (blue, D), Cep97 (blue, C) or CP110 (red, D). DNA, blue (B). Insets (B) show centrioles (dashed white boxes) at higher magnification. (C and D) GFP-Cep104 co-localizes with Cep97 and CP110 at distal tips of centriole pairs as a central spot within the mother centriole (appears as a ring in cross-section) and an adjacent spot marking the procentriole. Schematics of mother (M) and daughter (D) centriole configurations are shown (last column).

(E and F) Graphs show the percentage of centrioles (stained for Plp or Asl) that co-localize with either one or two spots of distal tip proteins (CP110, Cep97 and GFP-Cep104) in a Fly-FUCCI stable S2 line (E) or S2 cells pulsed for 20 min with EdU (F). The presence of two distal tip spots on a single centriole marks a duplicated mother-daughter centriole pair, which are present from the G1/S-phase transition through early mitosis. Note, by S-phase, nearly all centrioles contain distal tip proteins. $n = 50$ cells per replicate. Each experiment performed in triplicate. Error bars, SEM. See also Figures S1–S3, Data S1 and Video S1.

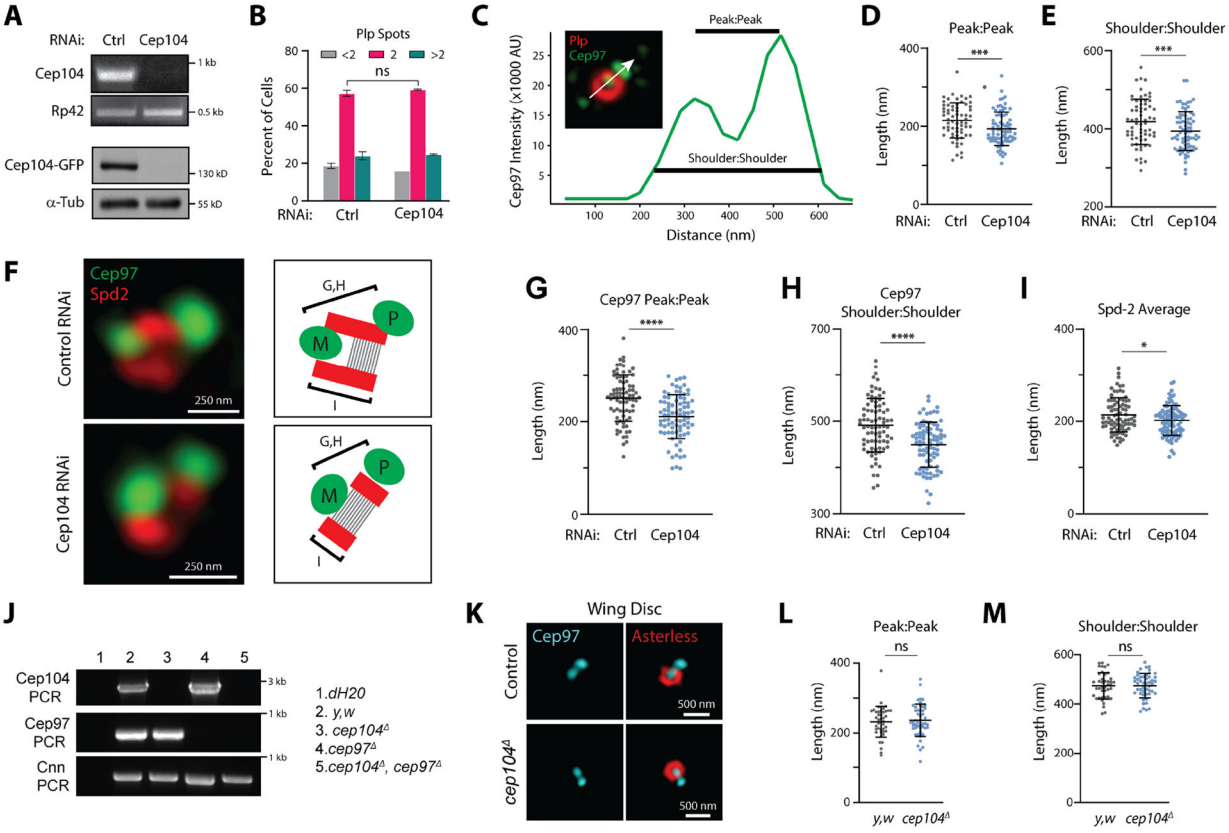

Figure 2. Cep104 is required for centriole growth in *Drosophila* S2 cells

(A) dsRNA targeting a Cep104 exon efficiently diminishes its mRNA and transgenic GFP-Cep104. (*Upper panel*) RT-PCR of Rp49 (control) and Cep104 from day 12 RNAi-treated S2 cells. (*Lower panel*) Anti-GFP immunoblots demonstrate effective depletion. α-tubulin, loading control.

(B) Cep104 depletion does not affect centriole number. RNAi-treated S2 cells were immunostained for Plp to mark centrioles, and the number of centrioles per cell was counted. n =100 cells in each of three experiments. Bars represent mean. Error bars, SEM.

(C) Centriole length measurements using 3D-SIM were performed by immunostaining for Plp or Asl (red) and Cep97 (green) in interphase cells to first identify optimally oriented mother-daughter pairs, where mother centrioles appeared as a ring with an orthogonally positioned procentriole/daughter. Graph shows Cep97 fluorescence intensity from a linescan through the centriole pair (arrow). Peak-to-peak and shoulder-to-shoulder (defined as a straight line drawn at 20% of the maximum Cep97 intensity) Cep97 measurements are presented.

(D and E) Whisker plots show centriole lengths in control and Cep104 RNAi-treated S2 cells. n = 65-control centrioles, 77-Cep104-RNAi centrioles combined from triplicate experiments. (D) Peak-to-peak lengths, control (215.0 nm ± 45.05), Cep104-RNAi (193.7 nm ± 42.75). (E) Shoulder-to-shoulder lengths, control (417.9 nm ± 58.05), Cep104-RNAi (394.0 nm ± 49.38).

(F) (Left panel) Centriole length measurements using 3D-SIM were in control and Cep104-depleted cells performed by immunostaining for Spd2 (red) and Cep97 (green).

Measurements were performed on only mother-procentriole pairs strictly oriented with the mother centriole in longitudinal section and the procentriole positioned on one side. Spd2 specifically labeled the mother centriole barrel appearing as two stripes. (Right panel) Schematics of mother (M) and procentriole (P) centriole configurations with regions of measurement indicated. For simplicity, the procentriole cartwheel is not shown.

(G and H) Whisker plots show centriole length in control and Cep104 RNAi-treated S2 cells. n = 82-control centrioles, 83-Cep104-RNAi centrioles combined from triplicate experiments. (G) Peak-to-peak lengths, control (250.9 nm ± 49.9), Cep104-RNAi (210.7 nm ± 47.1). (E) Shoulder-to-shoulder lengths, control (491.4 nm ± 58), Cep104-RNAi (449.3 nm ± 48.4). Measurements of Cep97 distance were performed as described in E and F but only on centriole pairs in with mothers in longitudinal orientation.

(I) Whisker plots show mother centriole length in control and Cep104 RNAi-treated S2 cells. n = 82-control centrioles (213.9 nm ± 36.9), 83-Cep104-RNAi centrioles (201.7 nm ± 32.2) combined from triplicate experiments. Measurements of mother centriole length (Spd2 stripes) were performed but only on mother-procentriole pairs with the mother in longitudinal orientation (described in Methods).

(J) DNA gel shows PCR amplicons from flies with the indicated genotypes: dH_2O (control), *y,w* (wild-type), and CRISPR-null *cep104*$^{\Delta}$, *cep97*$^{\Delta}$ and *cep104*$^{\Delta}$*cep97*$^{\Delta}$ double mutant. Cnn, positive control.

(K) 3D-SIM of centrioles in control (*y,w*) and *cep104*$^{\Delta}$ mutant wing discs immunostained for Cep97 blue and Asl (red).

(L and M) Whisker plots show centriole lengths in wing disc cells from control and *cep104*$^{\Delta}$ mutant fly lines. Measurements were done as described in (C). n = 41-control centrioles, 48-*cep104*$^{\Delta}$.

Error bars, SD unless indicated. Asterisks indicate significant differences: *, P <0.05; **, P <0.001; ***, P <0.0001; ns, not significant.

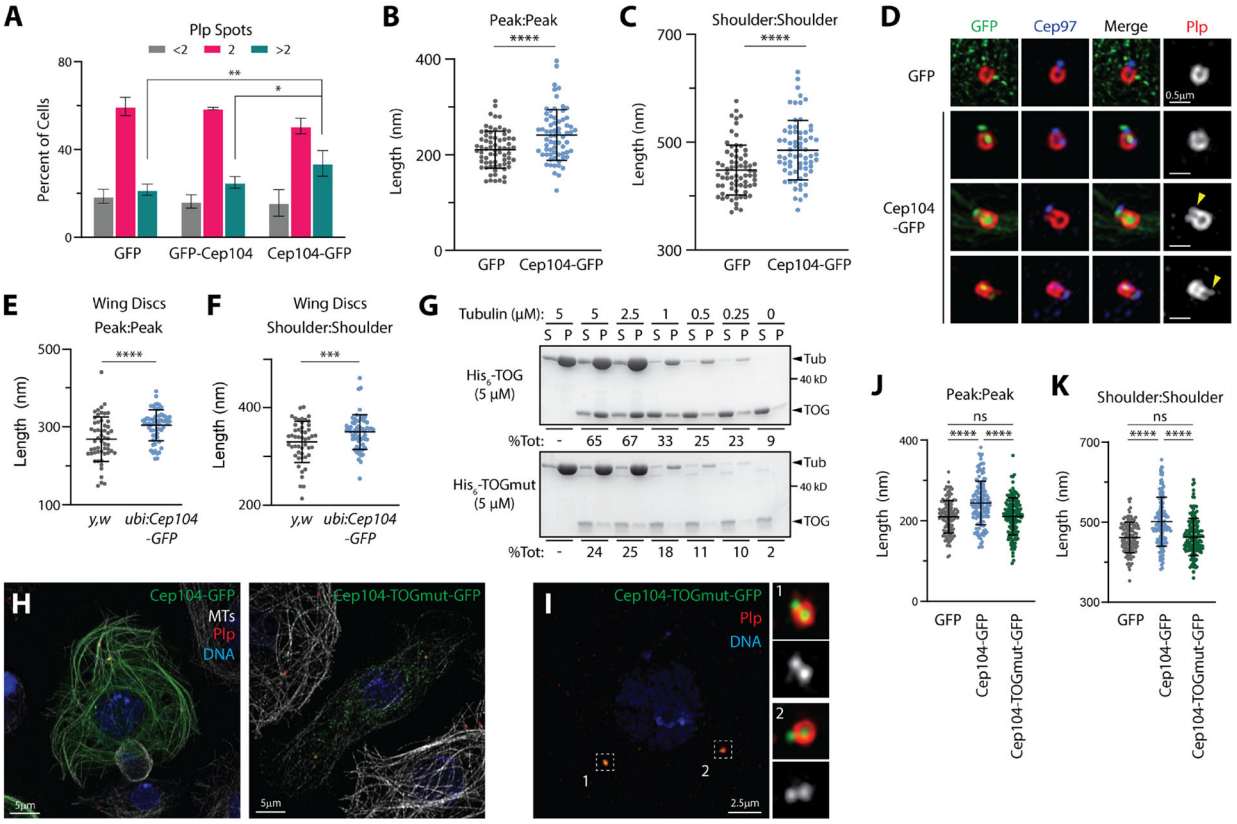

Figure 3. Cep104 promotes centriole elongation through its TOG domain

(A) Cep104 overexpression increases centriole number in S2 cells. GFP-Cep104 indicates N-terminal GFP and Cep104-GFP indicates C-terminal GFP. Cells were then immunostained for PLP and the number of centrioles per cell was counted. *n* =100 cells per replicate, performed in triplicate. Error bars, SEM.

(B and C) Whisker plots show centriole lengths in S2 cells overexpressing either control GFP or Cep104-GFP. *n* =70-GFP centrioles, 68-Cep104-GFP centrioles combined from triplicate experiments. (B) Peak-to-peak lengths, GFP (210.4 nm ± 38.93), Cep104-GFP (241.3 nm ± 52.98). (C) Shoulder-to-shoulder lengths, GFP (448.1 nm ± 46.31), Cep104-GFP (485.2 nm ± 54.85).

(D) Cep104 overexpression induces centriole elongation. 3D-SIM of S2 cells immunostained for Plp (red) and Cep97 (blue). Cep104-GFP (green). (Rows 1 and 2) Examples of normal duplicated centriole pairs. (Rows 3 and 4) Daughter centrioles show abnormal accumulation of Plp and longer growth (yellow arrowheads); mother centrioles shown in cross-section.

(E and F) Whisker plots show centriole lengths in wild-type or Cep104-GFP overexpressing wing discs. *n* =54-control centrioles (268.3 nm ± 56.9), 60-Cep104-GFP (304.2 nm ± 39.7) peak:peak and 49-shoulder-to-shoulder control centrioles (459.3 nm ± 84.53), 60-Cep104-GFP (499.5 nm ± 70.9).

(G) The TOG domain mutant (TOGmut) of Cep104 has decreased microtubule binding compared to wild-type TOG. Purified TOG or TOGmut was incubated with a varying concentration of taxol-stabilized microtubules, then microtubules were pelleted and the

supernatant (soluble) and pellet (co-sedimenting) fractions examined by Coomassie-stained SDS-PAGE to evaluate microtubule-binding. Lanes 1 and 2, no TOG. The percent total TOG (%Tot) in the pellet is shown below each gel. $n = 6$, 2 independent TOG preparations.
(H) S2 cells overexpressing high levels of Cep104-GFP (green) decorate microtubules of the interphase array and centrioles (left), whereas Cep104-TOGmut-GFP (green) appears instead as punctate cytoplasmic aggregates (right). Immunostained for Plp (red) and tubulin (white). DNA, blue.
(I) Microtubule binding is not required for Cep104's centriole distal tip localization. Cep104-TOGmut-GFP (green) localizes as 2 spots on Plp (red) foci. DNA, blue. Insets show centrioles (dashed boxes) at higher magnification.
(J and K) Whisker plots show centriole lengths in S2 cells overexpressing control GFP, WT-Cep104-GFP, and Cep104-TOGmut-GFP. $n = 135$-GFP centrioles, 132-Cep104-GFP, and 156-Cep104-TOGmut-GFP centrioles combined from triplicate experiments. (J) Peak-to-peak, GFP (209.8 nm ± 40.40), Cep104-GFP (244.3 nm ± 54.03), Cep104-TOGmut-GFP (210.8 nm ± 46.23). (K) Shoulder-to-shoulder, GFP (461.6 nm ± 38.17), Cep104-GFP (501.3 nm ± 61.27), Cep104-TOGmut-GFP (462.9 nm ± 46.52).
Error bars, SD unless indicated. Asterisks indicate significant differences: **, $P < 0.01$; ***, $P < 0.001$; ****, $P < 0.0001$; ns, not significant.

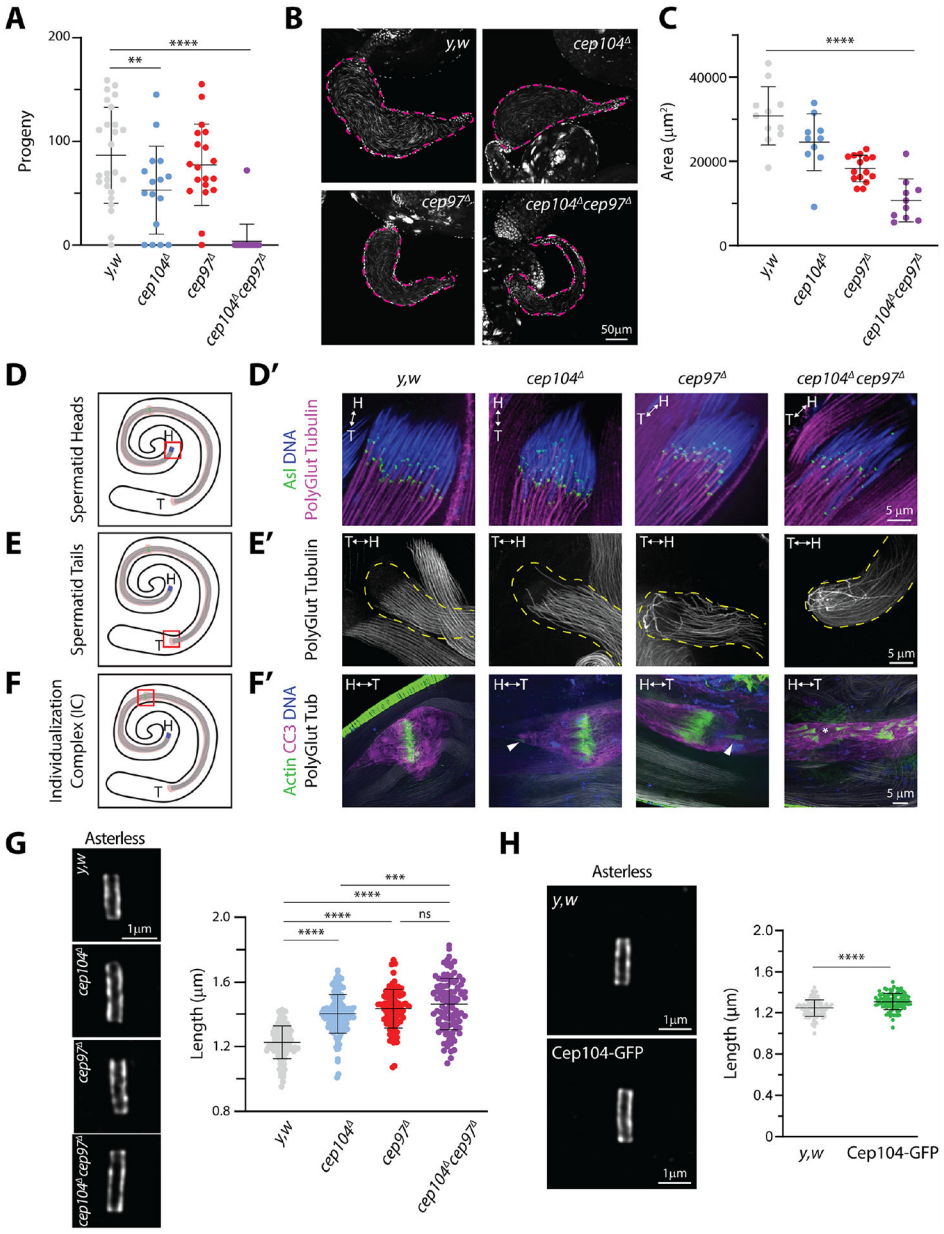

Figure 4. Cep104 and Cep97 play independent, synergistic functions in spermiogenesis but not in regulating the length of meiotic centrioles

(A) Male flies lacking Cep104 and Cep97 are almost entirely infertile. *n* =25-control, 16-*cep104*$^{\Delta}$, 19-*cep97*$^{\Delta}$, 19-*cep104*$^{\Delta}$*cep97*$^{\Delta}$.

(B and C) The DNA-stained seminal vesicles (dashed lines) of *cep104*$^{\Delta}$*cep97*$^{\Delta}$ males are reduced in size (B). Graph (C) shows measurements of seminal vesicle areas. *n* =11-control, 10-*cep104*$^{\Delta}$, 15-*cep97*$^{\Delta}$, 10-*cep104*$^{\Delta}$*cep97*$^{\Delta}$.

(D-F) *cep104*$^{\Delta}$*cep97*$^{\Delta}$ double mutants show severe defects in sperm individualization during late spermatocyte maturation. Cartoons mark regions of interest (red boxes) shown as magnified images (D'-F') within testes of the indicated genotypes. H↔T denotes head-to-tail axis of spermatids. (D' and E') Spermatid heads and tails (dashed lines) were stained for Asl (green) and/or poly-glutamylated tubulin (magenta or monochrome) to label axonemes.

cep104$^{\Delta}$*cep97*$^{\Delta}$ spermatid heads and tails are severely disorganized with fewer nuclei compared to single mutants. (F') Individualization complexes (IC) revealed by phalloidin labeling of actin (green) and immunostaining for CC3 (magenta) to label cystic bulges. Actin cones travel as a cluster towards spermatid tails with cone tips pointing backwards. In *cep104*$^{\Delta}$ and *cep97*$^{\Delta}$ mutants, lagging and leading actin cones were observed (arrowheads). However, in *cep104*$^{\Delta}$*cep97*$^{\Delta}$ double mutants, ICs were spread across a wide area with no distinguishable cystic bulge and actin cones of mixed orientation. DNA, blue.

(G) (Left) Lattice SIM images of spermatocyte centrioles in meiosis II immunostained for Asterless (Asl). (Right) Elimination of Cep104 or Cep97 or both results in similar increases in centriole length compared to control. *n* =119-control, 131-*cep104*$^{\Delta}$, 104-*cep97*$^{\Delta}$, 104-*cep104*$^{\Delta}$*cep97*$^{\Delta}$.

(H) Cep104-GFP overexpression increases centriole length in meiosis II. (Left) Lattice SIM images of Asterless immunostained centrioles. (Right) Graph shows centriole length measurements. *n* = 92-control, 8 testes; 92-ubi:Cep104-GFP, 6 testes.

Error bars, SD. Asterisks indicate significant differences: **, P<0.01; ***, P<0.001; **** P<0.0001; ns, not significant. See also Figures S4 and S5.

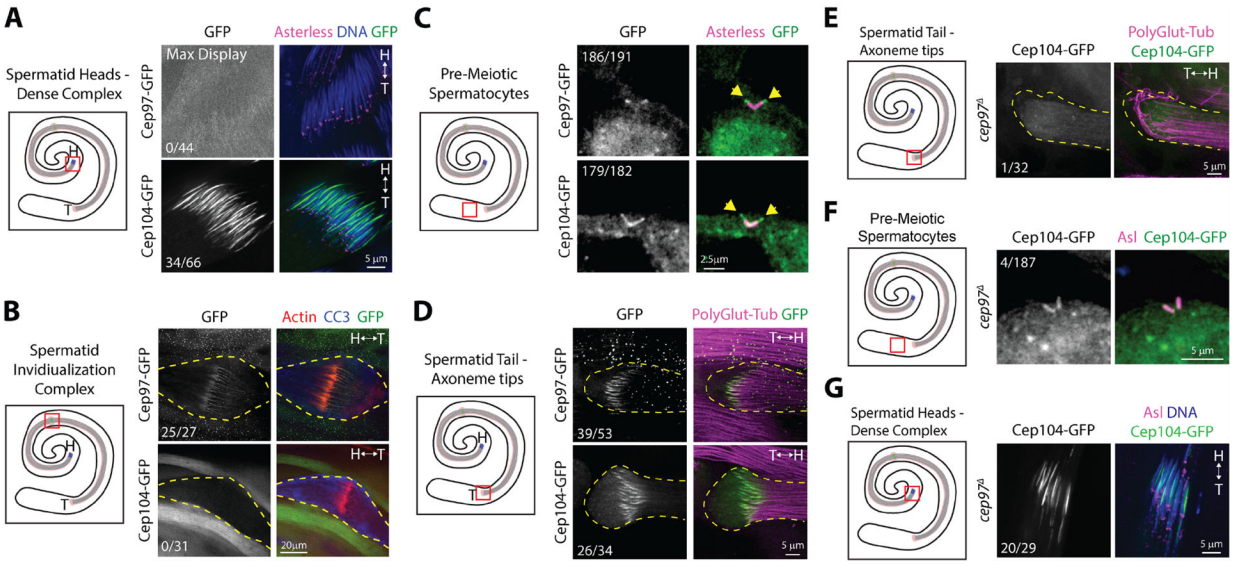

Figure 5. In fly testes, Cep104 localization is dependent on Cep97 only in those regions where Cep104 co-localizes with Cep97

(A-G) Cep104 is dependent on Cep97 for its localization to axonemal tips in spermatid tails and centriole distal tips in spermatocytes where they normally co-localize but is not dependent on Cep97 to target the dense complex in spermatid heads (needle stage) and centriole barrels in spermatocytes. Cep97 distinctly localizes to the IC. Cartoons (left) mark regions of interest (red boxes) shown as magnified images (right) within testes of the indicated genotypes and expressing either Cep97-GFP (green, A-D) or Cep104-GFP (green, A-G). Testes were immunostained for Asterless (Asl) (magenta; A, C, F, G), polyglutamylated tubulin (magenta; D, E) or actin (red; B) and CC3 (blue; B). DNA, blue (A, G). H↔T denotes head-to-tail axis of spermatids. The fraction of wild-type localizations of the indicated GFP-fusion protein in centrioles/cysts/ICs is shown; for example, the Cep104-GFP pattern at axoneme tips is observed in 76% of wild-type spermatid tails (D) but absent in 97% of *cep97*$^{\Delta}$ mutants (E).

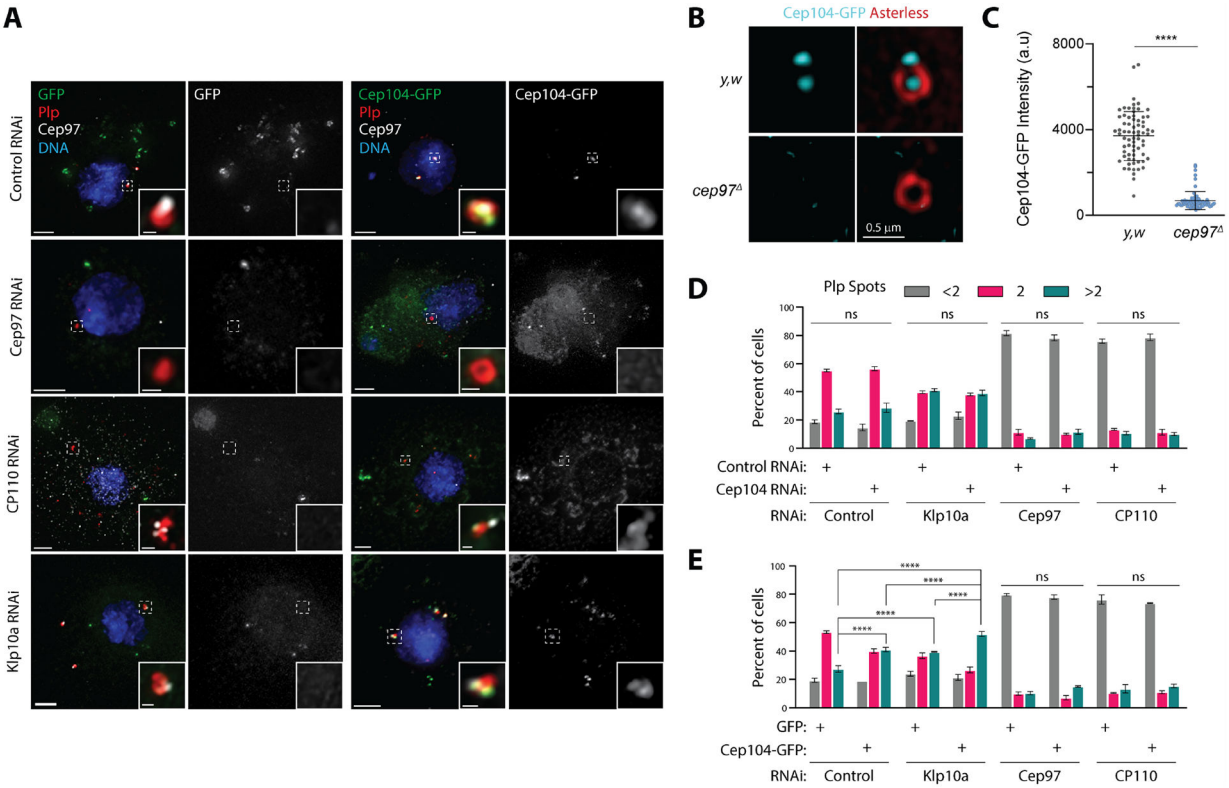

Figure 6. Cep104 is dependent on Cep97 for its localization to the distal tip of centrioles in somatic S2 cells and wing discs

(A) Cep97, but not CP110 or Klp10a, recruits GFP-Cep104 to centriole tips. RNAi-treated S2 cells expressing control GFP (green) or Cep104-GFP (green) were immunostained for Plp (red) to mark centrioles and Cep97 (white) to label distal tips. DNA, blue. Scale, 2.5 µm. Insets show boxes at higher magnification. Inset scale, 0.3 µm. (B) 3D-SIM of Cep104-GFP (cyan) on centrioles in control (*y,w*) and *cep97*$^{\Delta}$ mutant wing discs immunostained for Asterless (red).

(C) The fluorescence intensity of Cep104-GFP on wing disc centrioles is significantly diminished in *cep97*$^{\Delta}$ mutant flies. n =71-control, 71-*cep97*$^{\Delta}$. Error bars, SD. Asterisks indicate significant difference: ****, $P < 0.0001$.

(D and E) A functional interaction analysis of centriole distal tip proteins reveals that overexpression of Cep104 in Klp10a-depleted cells increase centriole number, indicating an increase in cells with centriole over-elongation. Double RNAi-treated S2 cells (D) or cells expressing GFP or Cep104-GFP (E) were immunostained for Plp, and the number of centrioles per cell was counted. n =100 cells in each of three experiments. Error bars, SEM. Asterisks indicate significant differences: ****, $P < 0.0001$.

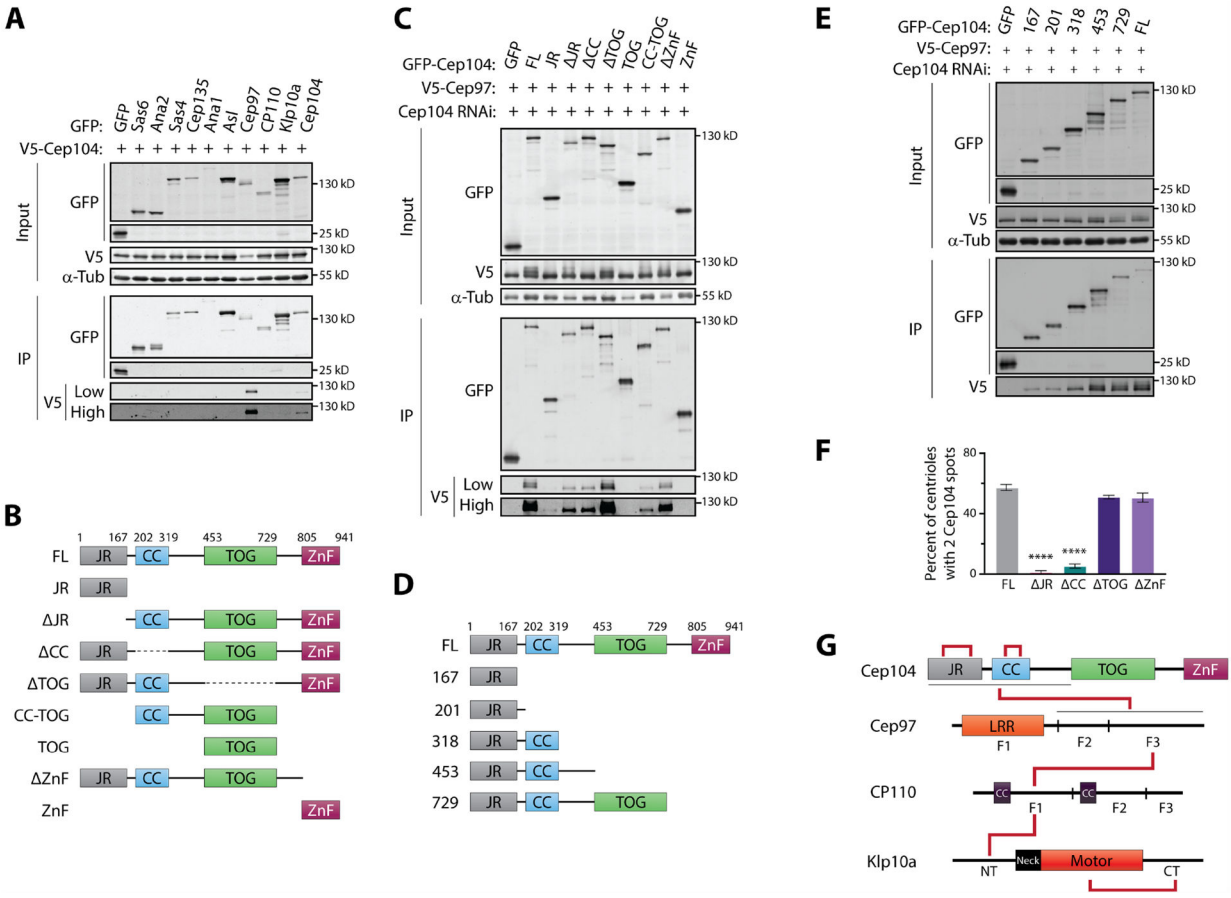

Figure 7. The centriole Distal Tip Complex is composed of Cep104-Cep97-CP110-Klp10a

(A) Cep104 binds only Cep97 and itself. S2 cells were co-transfected with the indicated plasmids and the next day induced to express for 24 h by the addition of 0.5 mM $CuSO_4$. Anti-GFP IPs were then prepared from clarified cell lysates, and Western blots of the inputs and IPs probed for GFP, V5, and α-tubulin (loading control). $n = 3$. Low, short exposure; high, long exposure.

(B) Schematics of the Cep104 truncation and deletion constructs used in (C). Dashed lines indicate deleted sequence.

(C) Cep104 binds Cep97 through its JellyRoll (JR) and Coiled-Coil (CC) domains. S2 cells depleted of endogenous Cep104 by RNAi targeting its 3'UTR were co-transfected with the indicated plasmids. IPs were performed as in (A) and blots of lysates probed with anti-GFP, V5 and α-tubulin. $n = 3$.

(D) Schematics of the Cep104 truncation constructs used in (E).

(E) Cep104 N-terminus (amino acids 1–453) is sufficient for maximal binding of Cep97. S2 cells were treated as described in (C). $n = 3$.

(F) The JR and CC domains are necessary for Cep104 to target the distal tips of centrioles. S2 cells were transfected with the indicated GFP-tagged constructs and then immunostained for Plp. Graph shows percentage of centrioles in GFP-positive cells associated with 2 Cep104 spots, indicating a distal tip localization of a duplicated centriole pair.

(G) Schematic shows sites of interaction (red lines) and self-association (red brackets) within components of the centriole Distal Tip Complex (DTC) based on IP analysis. LRR, leucine-rich repeat. See also Figures S6 and S7.

KEY RESOURCES TABLE

REAGENT or RESOURCE	SOURCE	IDENTIFIER
Antibodies		
Rabbit monoclonal anti-Cleaved caspase 3	Cell Signaling Technologies	#9664
Mouse monoclonal anti-polyglutamylated tubulin GT335	Adipogen	#AG-20B-0020-C100
Guinea pig anti-Spd2 antibody	Renata Basto (Institut Curie)	N/A
Alexa Fluor 488 conjugated secondary antibodies	Thermo Fisher Scientific	Variable host and target species
Mouse monoclonal anti-GFP JL-8 antibody	Thermo Fisher Scientific	Cat#NC9777966
Alexa Fluor 568 conjugated secondary antibodies	Thermo Fisher Scientific	Variable host and target species
Mouse monoclonal anti-V5 antibody	Thermo Fisher Scientific	Cat#R960–25
Mouse monoclonal anti-α-tubulin DM1a antibody	Sigma-Aldrich	Cat#T9026
Rabbit polyclonal anti-Cep104 antibodies	This study	N/A
Chicken polyclonal anti-Cep97 antibodies	This study	N/A
Guinea pig polyclonal anti-CP110 antibodies	This study	N/A
Rat polyclonal anti-Klp10a antibody	This study	N/A
IRDye 800CW goat anti-mouse IgG secondary antibody	Li-Cor	Cat#926–32210
IRDye 800CW donkey anti-chicken secondary antibody	Li-Cor	Cat#926–32218
IRDye 800CW donkey anti-guinea pig IgG secondary antibody	Li-Cor	Cat#926–32411
IRDye 800CW goat anti-rat IgG secondary antibody	Li-Cor	Cat#926–32219
IRDye 800CW goat anti-rabbit IgG secondary antibody	Li-Cor	Cat#926–32211
AlexaFluor 488 goat anti-chicken IgG	Thermo Fisher Scientific	Cat#A11039
AlexaFluor 488 goat anti-guinea pig IgG	Thermo Fisher Scientific	Cat#A11073
AlexaFluor 488 goat anti-rat IgG	Thermo Fisher Scientific	Cat#A11006
AlexaFluor 488 donkey anti-rabbit IgG	Thermo Fisher Scientific	Cat#A21206
Rhodamine Red-X AffiniPure donkey anti-rabbit IgG	Jackson Immunoresearch	Cat#711–295–152
Rhodamine Red-X AffiniPure goat anti-rat IgG	Jackson Immunoresearch	Cat#112–295–143
Cy5 AffiniPure Donkey anti-chicken IgY (IgG)	Jackson Immunoresearch	Cat#703–175–155
Cy5 AffiniPure Donkey anti-guinea pig IgG	Jackson Immunoresearch	Cat#706–175–148
Cy5 AffiniPure goat anti-mouse IgG	Jackson Immunoresearch	Cat#115–175–166

REAGENT or RESOURCE	SOURCE	IDENTIFIER
Alexa Fluor 647 conjugated secondary antibodies	Thermo Fisher Scientific	Variable host and target species
Bacterial and virus strains		
BL21(DE3)pLysS competent *E.coli*	Promega Corp	Cat#L1191
5-alpha competent *E.coli*	New England Biolabs	Cat#C29871
GC10 Competent Bacteria	Genesee Scientific	Cat #42–659 or Cat # 42–661
Chemicals, peptides, and recombinant proteins		
Neomycin G418	Thermo Fisher Scientific	Cat#J62671.03
Glutathione Agarose Resin	Gold Biotechnology	G-250–10
complete His-Tag Purification Resin	Roche	Cat#57356000
Affi-Gel 10 Gel	Bio-Rad	Cat#1536099
Amylose Resin	New England BioLabs	Cat#E8021S
Normal Goat Serum	Sigma Aldrich	Cat#G9023
Triton X-100	Thermo Fisher Scientific	Cat#BP151–500
Paraformaldehyde 16% Solution	Electron Microscopy Sciences	Cat#15710
488-conjugated streptavidin	Thermo Fisher Scientific	Cat#S11223
Biotin	Sigma-Aldrich	Cat#B4501
Dynabeads Protein A	Thermo Fisher Scientific	Cat#10001D
Dynabeads™MyOne™Streptavidin C1	Thermo Fisher Scientific	Cat#65001
IRDye® 800CW Streptavidin	Li-Cor	Cat#C91204–06
DAPI	Thermo Fisher Scientific	Cat#D1306
Vectashield	Vector Laboratories	Cat#H-1000
ProLong Glass antifade mountant	ThermoFisher Scientific	Cat#P36984
Phusion High-Fidelity DNA Polymerase	Thermo Fisher Scientific	Cat#F530L
Alexa Fluor™ 488 Phalloidin	Invitrogen	Cat#A12379
Aureobasidin A	Takara	Cat#630499
X-alpha-Gal	Takara	Cat#630463
Hoechst 33342	Life Technologies	Cat#H3570
Sf-900 II SFM	Gibco	Cat#10902–088
Penicillin Streptomycin Solution	Corning	Cat#30–002-CI
RNase-Free DNase	Qiagen	Cat#P79254

REAGENT or RESOURCE	SOURCE	IDENTIFIER
Phenylmethanesulfonyl fluoride	Sigma-Aldrich	Cat#P7626
Critical commercial assays		
T7 RiboMAX™ Large Scale RNA Production System	Promega	Cat#P1300
pENTR/D-TOPO Kit	Thermo Fisher Scientific	Cat#K2400–20
SuperScript III One-Step system	Invitrogen	Cat# 12574–018
Gateway LR Clonase	Thermo Fisher Scientific	Cat#11791043
RNeasy Mini Kit	Qiagen	Cat#75144
Deposited data		
Experimental models: Cell lines		
D. melanogaster: Cell line S2	Thermo Fisher Scientific	Cat#R69007
Experimental models: Organisms/strains		
Drosophila melanogaster: ubi-CP110 GFP	Rusan Lab	FBal0319930
Drosophila melanogaster: y,w	Gift from Mark Peifer, UNC Chapel Hill	N/A
Drosophila melanogaster: cep104$^{\Delta}$	This study	N/A
Drosophila melanogaster: cep97$^{\Delta}$	Gift From Alexander Dammermann – Max Perutz Labs, Vienna.	FBti0212678
Drosophila melanogaster: ubi-cep104::GFP	This study	N/A
Drosophila melanogaster: ubi-Cep97::GFP	Rusan Lab	Rusan Lab
Oligonucleotides		
Primer: dsRNA synthesis T7 RNA polymerase promoter sequence: TAATACGACTCACTA	This paper	N/A
5’ Cep104 gRNA F: CTTCGTTGGACCGACACTACTGGA	IDTDNA	N/A
5’ Cep104 gRNA R: AAACTCCAGTAGTGTCGGTCCAAC	IDTDNA	N/A
3’ Cep104 gRNA F: CTTCGAGGCGAACACCACGTTAA	IDTDNA	N/A
3’ Cep104 gRNA R: AAACTTTAACGTGGTGTTCGCCTC	IDTDNA	N/A
5’homology arm F: GTACTTCGCGAATGCGTCGAGATACCAATGCAGTACATCCTTCTTGTAGAGCCTGAAGGA	IDTDNA	N/A
5’ homology arm R: CGCTTCTGACCTGGGAAAACGTGAAGAATTGTTGACGTCGCGCCGTCAAAAGCGCACTAC	IDTDNA	N/A
3’ homology arm F: CGTATAATGTATGCTATACGAAGTTATAGGAAAGCGTACACTTAATCGATCTATTGGCCT	IDTDNA	N/A
3’ homology arm R: CTCGTCGGTCCCGGCATCCGATCCAATAGGAAAACACGCGACGGTCTTCAAAAAGGAGAG	IDTDNA	N/A
Cep104 CRISPR Screening F: TTGGAACACGTAGCCTTTGGACAC	IDTDNA	N/A
Cep104 CRISPR Screening R: TACTGGTGGTTCATCAAGCGTCTG.	IDTDNA	N/A
Cep97 PCR Screening F: CGCCTCCAATTATCGATAGACGTA	IDTDNA	N/A
Cep97 PCR Screening R: CTGTTTGGGTTAACAAAGCACAGT	IDTDNA	N/A
Cep104 PCR screening F: AGAGAGTCGTAATCGTTGTCTGGG	IDTDNA	N/A

REAGENT or RESOURCE	SOURCE	IDENTIFIER
Cep104 PCR screening R: AACTGACGCGAATAGAACTGCTCC	IDTDNA	N/A
Cnn PCR Screening F: TGTTAGGTTTTTCGAGGGG	IDTDNA	N/A
Cnn PCR Screening R: TCGTCTATGCTTTTGGACAG	IDTDNA	N/A
Klp10A1–278 F: CACCATGGACATGATTACGGTGGGGC	IDTDNA	N/A
Klp10A1–278 R: CTGATGGTCATCGACGGCCTGGC	IDTDNA	N/A
Klp10A$^{204–609}$ F: CACCATGGGCGCTAGTACCCGGCGATC	IDTDNA	N/A
Klp10A$^{204–609}$ R:CTCCTTGACACGATCCGCATAGCGCAGCG	IDTDNA	N/A
Klp10A$^{610–805}$ F: CACCATGCTGGTGGTCAAGGATATCGTCGAAG	IDTDNA	N/A
Klp10A$^{610–805}$ R: ACGCTTGCCATTCGGCGAATTGAAGC	IDTDNA	N/A
Klp10A$^{1–805}$ F: CACCATGGACATGATTACGGTGGGGC	IDTDNA	N/A
Klp10A$^{1–805}$ R: ACGCTTGCCATTCGGCGAATTGAAGC	IDTDNA	N/A
Cep104$^{1–201}$ F: CACCATGGCTAAGAAAATA CCTTTTAACGTGGTGTTCG	IDTDNA	N/A
Cep104$^{1–201}$ R: CTCCTCCACATACATGGAGAAAAGCAGGTCATC	IDTDNA	N/A
Cep104$^{202–713}$ F: CACCATGTCAATAGTGCAGACCATCCGAGAGTTGG	IDTDNA	N/A
Cep104$^{202–713}$ R: ATCCAACTTGTCAAATTCGGTGAAGAGTTGGCGGTAC	IDTDNA	N/A
Cep104$^{714–941}$ F: CACCATGCTGGACCGCAAGCAGGAG	IDTDNA	N/A
Cep104$^{714–941}$ R: ATTTGACTTCTTGAGATTCCTCTTGCGTATATTCCCGGGACAG	IDTDNA	N/A
Cep104$^{1–941}$ F: CACCATGGCTAAGAAAATACCTTTTAACGTGGTGTTCG	IDTDNA	N/A
Cep104$^{1–941}$ R: ATTTGACTTCTTGAGATTCCTCTTGCGTATATTCCCGGGACAG	IDTDNA	N/A
RT-PCR primer Cep104-For: CTTCCCATCCTGGTCTTCGG	IDTDNA	N/A
RT-PCR primer Cep104-Rev: CTTGCGGTCCAGATCCAACT	IDTDNA	N/A
RT-PCR primer Rp49-For: ATCCGCCCAGCATACAGG	IDTDNA	N/A
RT-PCR primer Rp49-Rev: CTCGTTCTCTTGAGAACGCAG	IDTDNA	N/A
Recombinant DNA		
pMT/V5-HisC	Life Technologies	Cat#K4120–01
Fly-FUCCI live cell cycle reporter system: Ac-5-STABLE2-RFP-NLS-CycB(1–266)_GFP-E2F1(1–230)_neo	Addgene	Cat#73164
pU6-BbsI-chiRNA	Addgene	Plasmid #45946
pUWG	DGRC	1284
pGBKT7	Takara	Cat #: 630443
pGADT7	Takara	Cat #: 630442
pMAL-c2	Addgene	Cat#75286
pGEX-6p2	Addgene	Cat#27–4598–01
pET28a	Addgene	Cat#69864–3
pMal c2x MBP-Klp10a 1–201	This study	N/A
pET28A His_6-Cep97 514–806	This study	N/A

REAGENT or RESOURCE	SOURCE	IDENTIFIER
pET28A His_6-Cep104-TOG	This study	N/A
pET28A His_6-Cep104-TOGmut	This study	N/A
pMal c2x MBP-CP110 326–549	This study	N/A
pGex 6p2 GST-Cep104 730–941	This study	N/A
pGex 6p2 GST-Klp10a 1–201	This study	N/A
pGex 6p2 GST- Cep97 514–806	This study	N/A
pGex 6p2 GST- CP110 326–549	This study	N/A
pFlc-I Cep97 5'–3' UTR Fusion	This study	N/A
pEB1-TagRFP	Gift from Stephen Rogers, UNC Chapel Hill	N/A
pMT/V5 His C GFP-Cep104	This study	N/A
pMT/V5 His C Cep104-GFP	This study	N/A
pMT/V5 His C Cep104-TOGmut-GFP	This study	N/A
pMT/V5 His C GFP-Sas6	Rogers Lab	Rogers Lab
pMT/V5 His C Ana2-GFP	Rogers Lab	Rogers Lab
pMT/V5 His C Cep135-GFP	Rogers Lab	Rogers Lab
pMT/C5 His C GFP-Ana1	This study	N/A
pMT/V5 His C Asl-GFP	Rogers Lab	Rogers Lab
pMT/V5 His C Cep97-GFP	This study	N/A
pMT/V5 His C CP110-S-GFP	This study	N/A
pMT/V5 His C CP110-L-GFP	This study	N/A
pMT/V5 His C Klp10a-GFP	This study	N/A
pMT/V5 His C GFP	Rogers Lab	Rogers Lab
pMT/V5 His C GFP-Cep104-JR	This study	N/A
pMT/V5 His C GFP-Cep104-ΔJR	This study	N/A
pMT/V5 His C GFP-Cep104-ΔCC	This study	N/A
pMT/V5 His C GFP-Cep104-ΔTOG	This study	N/A
pMT/V5 His C GFP-Cep104-TOG	This study	N/A
pMT/V5 His C GFP-Cep104-CC-TOG	This study	N/A
pMT/V5 His C GFP-Cep104-ΔZnF	This study	N/A
pMT/V5 His C GFP-Cep104-ZnF	This study	N/A
pMT/V5 His C GFP-Cep104–201	This study	N/A
pMT/V5 His C GFP-Cep104–318	This study	N/A
pMT/V5 His C GFP-Cep104–453	This study	N/A
pMT/V5 His C GFP-Cep104–729	This study	N/A
pMT/V5 His C V5-miniTurbo-NES	This study	N/A
pMT/V5 His C V5-Cep97-miniTurbo	This study	N/A
pMT/V5 His C V5-Cep104	This study	N/A

REAGENT or RESOURCE	SOURCE	IDENTIFIER
pMT/V5 His C V5-Cep97	This study	N/A
pMT/V5 His C V5-Klp10a	This study	N/A
pMT/V5 His C V5-CP110-S	This study	N/A
pMT/V5 His C V5-CP110-L	This study	N/A
pMT/V5 His C Cep97-F1-GFP	This study	N/A
pMT/V5 His C Cep97-F2-GFP	This study	N/A
pMT/V5 His C Cep97-F3-GFP	This study	N/A
pMT/V5 His C Cep97-ΔF1-GFP	This study	N/A
pMT/V5 His C Cep97-ΔF2-GFP	This study	N/A
pMT/V5 His C Cep97-ΔF3-GFP	This study	N/A
pMT/V5 His C CP110-F1-GFP	This study	N/A
pMT/V5 His C CP110-F2-GFP	This study	N/A
pMT/V5 His C Klp10a-NT-GFP	This study	N/A
pMT/V5 His C Klp10a-Neck-GFP	This study	N/A
pMT/V5 His C Klp10a-Motor-GFP	This study	N/A
pMT/V5 His C Klp10a-CT-GFP	This study	N/A
pMT/V5 His C Klp10a-ΔNT-GFP	This study	N/A
pMT/V5 His C Klp10a-ΔNeck-GFP	This study	N/A
pMT/V5 His C Klp10a-ΔMotor-GFP	This study	N/A
pMT/V5 His C Klp10A-ΔCT-GFP	This study	N/A
pMT/V5 His C Klp10A-N/M-GFP	This study	N/A
pMT/V5 His C Klp10A-ΔN/M-GFP	This study	N/A
Software and algorithms		
Prism 7	GraphPad	www.graphpad.com/scientificsoftware/prism/
FlyCRISPR design tool	University of Wisconsin	www.flycrispr.org
Elements	Nikon	www.microscope.healthcare.nikon.com/products/software/nis-elements/viewer
FIJI / ImageJ	NIH	www.fiji.sc
Zen Black	Zeiss	www.micro-shop.zeiss.com/en/us/softwarefinder/software-categories/zen-black
Adobe Illustrator	Adobe	www.adobe.com/in/products/illustrator.html
Adobe Photoshop	Adobe	www.adobe.com/products/photoshop.html

REAGENT or RESOURCE	SOURCE	IDENTIFIER
Softworx	Cytiva	https://download.cytivalifesciences.com/cellanalysis/download_data/softWoRx/7.2.1/SoftWoRx.htm